Chapter 5

Physics Studies with Tracks, B mesons, and taus

5.1 Benchmark Channels: study of the decay $B_s \to J/\psi\phi$

5.1.1 Introduction

The decay $B_s^0 \to J/\psi\,\phi \to \mu^+\mu^- K^+ K^-$ is of particular interest, since it allows to study many properties of the B_s^0 system, such as the differences between the widths and the masses of the two weak eigenstates, B_s^H and B_s^L. Contrary to the B^0 system, the difference between the widths $\Delta\Gamma_s$ of the two weak eigenstates is expected to be large, with a relative difference $\Delta\Gamma_s/\bar{\Gamma}_s$ predicted to be in the order of 10% in the Standard Model. The first measurement from CDF ($\Delta\Gamma_s/\bar{\Gamma}_s = (65\,^{+25}_{-33} \pm 1)\%$ [127]) and the new preliminary result from DØ ($\Delta\Gamma_s/\bar{\Gamma}_s = (15 \pm 10\,^{+3}_{-4})\%$ [128]) have discrepancies between the two measured values themselves and with the Standard Model prediction. It is only very recently that a first measurement of the mass difference, Δm_s, has been performed at CDF. Time-integrated measurements are not possible, as the time-integrated mixing probability χ saturates at a value of 0.5 for large mass differences, and in time-dependent measurements, the high mass difference generates very rapid oscillations. As in the B_s^0 system the ratio $\Delta m_s/\Delta\Gamma_s$ depends on the ratio $|V_{cb}V_{cs}|/|V_{tb}V_{ts}|$, which is quite well known, and on QCD corrections, a measurement of $\Delta\Gamma_s$ would therefore yield an independent measurement of Δm_s. With the measurement already performed in the B^0 system, the ratio between the mixing parameters of the B^0 and B_s^0 could provide a measurement of the ratio $|V_{ts}|/|V_{td}|$.

Furthermore, this decay provides one of the best ways to determine the height of the Unitarity Triangle, η in the Wolfenstein parametrisation. At first order of the Wolfenstein parametrisation, the CP-violating weak phase $\phi_{CKM} = [\arg(V_{cs}^* V_{cb}) - \arg(V_{ts}^* V_{tb})]$, measured in the rate asymmetry, cancels, and higher order terms have to be taken, yielding a weak phase $\phi_{CKM} = 2\lambda^2\eta$. The weak phase is therefore expected to be very small, of the order of 0.03. The measurement of a significantly larger phase would indicate contributions from non-Standard Model processes.

Because of the relative orbital angular momentum between the decay products, the $J/\psi\,\phi$ final state is an admixture of CP-even and CP-odd states, and the total rate asymmetry suffers from a partial cancellation. As the CP-even and CP-odd components have different angular dependences, an analysis of the angular correlation of the decay will allow to separate the two states, thereby permitting to access the different parameters.

With a total B production cross section at $\sqrt{s} = 14$ TeV expected to be as high as $500\,\mu$b, a substantial number of fully reconstructed B_s^0 candidates can be expected. Nevertheless, a

high background has to be dealt with. The main sources of backgrounds identified are those containing a J/ψ decaying to two muons susceptible to satisfy the Level-1 trigger requirements.

The decay $B_s^0 \to J/\psi\,\phi$ is chosen as a benchmark channel since it is representative of exclusive B physics studies. It allows to study the capability of CMS to identify, select and fully reconstruct the decay of the B_s^0, which presents a significant challenge due to its relatively low momentum and high background. In addition, the measurement of the width difference $\Delta\Gamma_s$ on a sample of untagged $B_s^0 \to J/\psi\,\phi \to \mu^+\mu^- K^+K^-$ candidates using a maximum likelihood fit of the time dependent angular distribution can be attempted.

5.1.2 Event generation

In addition to the signal itself, the main backgrounds identified have been simulated with low luminosity pile-up ($\mathcal{L} = 2 \times 10^{33}\,\mathrm{cm}^{-2}\,\mathrm{s}^{-1}$). Kinematic requirements were applied in order to ensure that a significant fraction of the generated events would fulfil the Level-1 trigger requirements and that the final state particles are within the acceptance of the tracker ($|\eta| < 2.5$). The transverse momentum of the muons is thus required to be above 3 GeV/c for muons in the barrel ($|\eta| < 1.2$) and 2 GeV/c elsewhere. For the signal, the momenta of the kaons are required to be above 0.8 GeV/c.

For the samples composed of events with decays of B hadrons, $b\bar{b}$ pairs were generated with PYTHIA 6.215. The MSEL=1 card was used in order to correctly reproduce the three different contributions to the total cross section (parton fusion, flavour excitation, and gluon splitting). The fragmentation of the b quark is performed by PYTHIA and the subsequent decay of the B hadron is performed using the SIMUB generator [129], a dedicated B physics event generator. The decay $B_s^0 \to J/\psi\,\phi$ has to be performed with SIMUB, since PYTHIA does not take into account the angular distributions of the final decay products.

One of the b quarks in the event is forced to hadronise to a B_s^0 or $\bar{B}_s^0$ meson and to decay through the complete decay chain. With the kinematic requirements, using the world-average branching ratios for the decays of the B_s^0, J/ψ and ϕ mesons [54], the cross section is predicted to be $\sigma(B_s^0 \to J/\psi\,\phi \to \mu^+\mu^- K^+K^-) = 74 \pm 27\,\mathrm{pb}$.

The inclusive decays of B hadrons to final states with a J/ψ resonance are expected to be the most important background for the measurement. These were simulated using PYTHIA, since no detailed simulation of angular distributions of the final decay products is needed. In order to increase the number of events similar to the signal events, a pair of oppositely charged particles with $p_\mathrm{T} > 0.5\,\mathrm{GeV/c}$ and $|\eta| < 2.5$ forming a fake ϕ candidate is required in a region ($|\Delta\eta| < 1.5, |\Delta\varphi| < 1.5$) around the J/ψ direction and with an invariant mass within 30 MeV/c^2 of the world-average ϕ mass. In addition, this fake ϕ candidate is required to form a fake B_s^0 candidate with an invariant mass within 300 MeV/c^2 of the world-average B_s^0 mass. The cross section, including the kinematic requirements and branching-fractions, is estimated to be $\sigma(b \to J/\psi X) = 3.20 \pm 0.3\,\mathrm{nb}$.

Furthermore, a sample of $B^0 \to J/\psi\,K^{*0} \to \mu^+\mu^-\,K^+\pi^-$ events were simulated, since this final state can be misidentified as a $B_s^0 \to J/\psi\,\phi$ decay. In addition, this decay has a similar differential decay rate [130, 131] to the studied B_s^0 decay. The B^0 decay is simulated with SIMUB, where one of the b quarks in the event is forced to hadronise to a B^0 or $\bar{B}^0$ meson, and to decay through the complete decay chain. With the kinematic requirements, and using the world-average branching ratios, the cross section is predicted to be $\sigma(B^0 \to J/\psi\,K^{*0} \to$

Table 5.1: Values used for the mixing parameters, decay amplitudes, strong and weak phases in the simulation of the $B_s^0 \to J/\psi\,\phi$ and $B^0 \to J/\psi\,K^{*0}$ Monte Carlo sample.

Parameter	$B_s^0 \to J/\psi\,\phi$	$B^0 \to J/\psi\,K^{*0}$
$\tau = 1/\bar{\Gamma}$	1.405×10^{-12} s	1.528×10^{-12} s
$\Delta\Gamma/\bar{\Gamma}$	-0.2	0
Δm	17.8 ps^{-1}	0.509 ps^{-1}
$\lvert A_0(0)\rvert^2/\Gamma$	0.570	0.570
$\lvert A_\parallel(0)\rvert^2/\Gamma$	0.217	0.217
$\lvert A_\perp(0)\rvert^2/\Gamma$	0.213	0.213
δ_1	π	π
δ_2	0	0
ϕ	-0.04	0

$\mu^+\mu^-\,K^+\pi^-) = 366 \pm 22\,\mathrm{pb}$.

The uncertainties quoted on the estimates above do not include the uncertainties on the total $b\bar{b}$ cross section at LHC energies, the b fragmentation functions, the transverse momentum distribution of b quarks, and the uncertainties introduced by using the model of $b \to J/\psi X$ decays in PYTHIA. However, since both the signal and background are proportional to the same $b\bar{b}$ cross section, the signal-to-background ratio is unaffected by the corresponding uncertainty. The parameters used in the simulation of the $B_s^0 \to J/\psi\,\phi$ and $B^0 \to J/\psi\,K^{*0}$ decays are given in Table 5.1.

The direct production of J/ψ mesons is an important background at trigger level. Measurements at the Tevatron [132] have shown that predictions of the colour-singlet model, which is presently the one implemented in the PYTHIA generator, underestimate the measurements by several orders of magnitude. Perturbative QCD is used in this model to generate $c\bar{c}$ pairs, which then hadronise to a charmonium state in a non-perturbative way.

The observed discrepancy has led to a different approach [133], which has been implemented in a modified version of PYTHIA 6.225, tuned on Tevatron data. A $c\bar{c}$ pair is first formed taking into account all perturbative QCD diagrams, regardless of the final colour state. The $c\bar{c}$ state is then transformed into a colour-singlet by non-perturbative processes, such as the emission of a soft gluon.

This version of PYTHIA has been used to simulate a sample of J/ψ decaying to two muons for background studies. The J/ψ production cross section is calculated to be $141\,\mu$b. Taking the $J/\psi \to \mu^+\mu^-$ branching ratio and the kinematic requirements into account, a cross section of 310 ± 5 nb is expected. Only the statistical uncertainty is quoted and used; the large uncertainties on the total cross section for J/ψ production and on the p_T distribution are not included.

5.1.3 Trigger selection

5.1.3.1 The Level-1 trigger

The B_s^0 decay chain is selected at Level-1 by the dimuon trigger stream. At low luminosity it is foreseen [75] to use an identical threshold of 3 GeV/c on the transverse momentum of each muon, still keeping a low bandwidth occupancy of 0.9 kHz. Such a low p_T threshold ensures a very high selection efficiency on this channel, with a rate low-enough to allow the use of

lower quality muon candidates in the endcap region, recovering full geometrical acceptance of the muon detector up to $|\eta| < 2.4$. For this decay, two of the identified muons are required to have opposite charge.

5.1.3.2 The High-Level trigger

In the HLT, the signal events are identified by doing a full reconstruction of the B_s^0 decay, imposing invariant mass and vertex constraints. Indeed, at this stage, tracks can be reconstructed in the tracker in restricted (η, ϕ) regions via a partial reconstruction algorithm, where only the first 5 hits are used [7, Section 6.4.3.2]. To define the tracking regions, the primary (interaction) vertex is first identified and reconstructed using only hits in the Pixel detector, with the "Divisive Method" described in reference [134]. Since the primary vertex of $b\bar{b}$ events involves low momentum tracks, the three vertex candidates with the highest sum of the p_{T}^2 of the tracks, which is the default selection criterion, have to be retained in order to achieve a good efficiency.

For the muons, the tracking regions are chosen around the direction of the muons identified at Level-1. Since no link to the muon detectors can be done at this stage, all track pairs of opposite charge for which the invariant mass is within $150\,\mathrm{MeV/c^2}$ of the world-average J/ψ mass are retained. The resolution on the invariant mass of the J/ψ meson is found to be $51\,\mathrm{MeV/c^2}$. In addition, the p_{T} of each muon is required to be above $2.5\,\mathrm{GeV/c}$ in $|\eta| < 1.2$ or $2\,\mathrm{GeV/c}$ in $|\eta| \geq 1.2$, and the p_{T} of the J/ψ candidate above $4\,\mathrm{GeV/c}$. To remove the prompt J/ψ background, the two muon candidates are then fitted to a common decay vertex. The χ^2 of the fit is required to be below 10 and the significance of the transverse decay length is required to be above 3. Furthermore, the transverse momentum of the J/ψ candidate is required to be nearly parallel to its flight path in the transverse plane, since the J/ψ mesons produced in the decays of B_s^0 mesons are collimated around the direction of the B_s^0 meson by the relativistic boost. The cosine of the angle between the reconstructed momentum vector and the vector pointing from the production to the decay vertex is thus required to be larger than 0.9.

To reconstruct the kaons, a tracking region is chosen around the direction of each J/ψ candidate. Assigning the kaon mass to the reconstructed tracks, all oppositely charged track pairs for which the invariant mass is within $20\,\mathrm{MeV/c^2}$ of the world-average mass of the ϕ meson are retained, for a resolution on the invariant mass of the ϕ meson of $4.5\,\mathrm{MeV/c^2}$. The p_{T} of each of the kaon tracks is required to be above $0.7\,\mathrm{GeV/c}$, the p_{T} of the ϕ candidate above $1\,\mathrm{GeV/c}$ and the p_{T} of the B_s^0 candidate above $5\,\mathrm{GeV/c}$. With the two muon candidates, the four-track invariant mass is required to be within $200\,\mathrm{MeV/c^2}$ of the world-average mass of the B_s^0 meson. The resolution on the invariant mass of the B_s^0 meson is found to be $65\,\mathrm{MeV/c^2}$. Here as well, a vertex fit of the four tracks is performed, imposing similar requirements as above.

The distribution of the invariant mass of the candidates after the HLT requirements is shown in Figure 5.1 (left). The efficiencies for the different criteria, which include the respective reconstruction efficiencies, are given in Table 5.2 for the signal and the different background samples, together with the estimated rate. The total rate for this selection is well below 1 Hz, and a yield of approximately $456'000$ signal events can be expected within $30\,\mathrm{fb}^{-1}$ of data.

Table 5.2: Trigger selection efficiencies for the signal and background (defined with respect to the number of generated events) after each requirement, and estimated HLT rate.

Requirement	Signal	Background		
	$B_s^0 \to J/\psi\,\phi$	Inclusive $b \to J/\psi X$	$B^0 \to J/\psi\,K^{*0}$	Prompt J/ψ
Level-1	$45.76(6)\%$	$38.25(13)\%$	$46.91(13)\%$	$36.91(12)\%$
HLT - J/ψ selection	$28.69(7)\%$	$21.91(11)\%$	$30.28(12)\%$	$0.65(2)\%$
HLT - ϕ selection	$20.50(6)\%$	$1.23(3)\%$	$0.961(26)\%$	$0.0007(7)\%$
HLT rate (Hz)	0.03034(8)	0.0792(18)	0.0077(2)	0.002(2)

5.1.4 Offline selection and reconstruction

The first step in the offline selection is similar to the HLT selection, with the difference that the complete information from the detector is available. Candidates are reconstructed by combining two muons of opposite charge with two further tracks of opposite charge. As CMS does not possess a particle identification system suitable for this measurement, all measured tracks have to be considered as possible kaon candidates, which adds a substantial combinatorial background. At this stage, only loose requirements are applied, which are tightened after a kinematic fit.

First, all muons in the event are reconstructed using the global muon reconstruction algorithm [7, Section 9.1.3]. This algorithm is not fully efficient for low-p_{T} muons from J/ψ decays, being more suited to the reconstruction of high-p_{T} muons. Therefore, all tracks are reconstructed with the standard track reconstruction algorithm [7, Section 6.5]. Track-pairs of opposite charge for which the invariant mass is within $120\,\mathrm{MeV/c^2}$ of the world-average J/ψ mass are retained as a J/ψ candidate. The p_{T} of each muon is required to be above $3\,\mathrm{GeV/c}$ in $|\eta| < 1.2$ or $2\,\mathrm{GeV/c}$ in $|\eta| \geq 1.2$, and the p_{T} of the J/ψ candidate above $4\,\mathrm{GeV/c}$. The muon identification algorithm which uses information from the muon detector [7, Section 9.2.1.2], is applied to both tracks forming the J/ψ candidate. A J/ψ candidate is confirmed if both tracks share more than half of their hits in the silicon tracker with the muon tracks reconstructed by the global muon reconstructor, or if their compatibility score returned by the muon identification algorithm is greater than 0.1.

To reconstruct the ϕ meson, all tracks reconstructed with the standard track reconstruction algorithm are used. Requiring the p_{T} of each track to be above $0.8\,\mathrm{GeV/c}$ and assigning a kaon mass to the thus reconstructed tracks, all oppositely charged track pairs for which the invariant mass is within $20\,\mathrm{MeV/c^2}$ of the world-average mass of the ϕ meson are retained. The p_{T} of the ϕ candidate is required to be above $1\,\mathrm{GeV/c}$, and the p_{T} of the B_s^0 candidate above $5\,\mathrm{GeV/c}$.

A kinematic fit [135] is then made, where the four tracks are constrained to come from a common vertex and the invariant mass of the two muons is constrained to be equal to the mass of the J/ψ. Since the natural width of the ϕ meson is of the same order as the resolution due to the reconstruction, no mass constraint is applied to the two kaon tracks. With this fit, a resolution on the invariant mass of the B_s^0 meson of $14\,\mathrm{MeV/c^2}$ is found. The confidence level of the fit is required to be greater than 1×10^{-3} (seven degrees of freedom). The invariant mass of the two kaons is required to be within $8\,\mathrm{MeV/c^2}$ of the world-average mass of the ϕ meson. Finally, the cosine of the angle between the reconstructed momentum vector of the B_s^0 candidate and the vector pointing from the production to the decay vertex is required to

Table 5.3: Offline selection efficiencies for the signal and background (defined with respect to the number of generated events) after each requirement.

Requirement	Signal	Background		
	$B_s^0 \to J/\psi\,\phi$	$b \to J/\psi X$	$B^0 \to J/\psi\,K^{*0}$	Prompt J/ψ
HLT selection	20.50(6) %	1.23(3) %	0.937(14)%	0.0007(7) %
Reconstruction + Basic p_{T} req.	18.15(5) %	0.63(2) %	0.675(12) %	0.0007(7) %
Muon Identification	17.89(5) %	0.585(19) %	0.636(11) %	0.0007(7) %
Kinematic fit χ^2 req.	16.58(5) %	0.282(14) %	0.503(10) %	0.0007(7) %
Pointing constraint	16.48(5) %	0.258(13) %	0.497(10) %	–
ϕ mass req.	14.65(5) %	0.113(13) %	0.202(10) %	–

Table 5.4: Expected cross sections for the signal and background, after each requirement, with number of expected events.

	Signal	Background		
	$B_s^0 \to J/\psi\,\phi$	Inclusive $b \to J/\psi X$	$B^0 \to J/\psi\,K^{*0}$	Prompt J/ψ
$\sigma \times \mathrm{BR}$	2.87 ± 1.07 nb	682 ± 64 nb	20.4 ± 1.7 nb	$141\ \mu$b
Kin. preselection	74 ± 27 pb	3.20 ± 0.3 nb	366 ± 22 pb	176 ± 2 nb
Level-1	34 ± 12 pb	1.22 ± 0.11 nb	172 ± 10 pb	65 ± 1 nb
HLT	15.2 ± 5.5 pb	39.4 ± 3.8 pb	3.52 ± 0.21 pb	1.2 ± 1.2 pb
Offline	10.9 ± 4.0 pb	3.62 ± 0.54 pb	0.74 ± 0.06 pb	–
Events per 30 fb^{-1}	327 000	108 500	22 200	-

be larger than 0.95. The distribution of the invariant mass of the candidates after all selection requirements is shown in Figure 5.1 (right).

The primary vertex is not used at this stage, since the efficiency of the standard primary vertex finder [7, Section 6.6.4], which uses all fully reconstructed tracks, is 92%, and drops to 83% if the vertex is required to be within 500 μm from the simulated vertex. In order to prevent this unnecessary loss of efficiency, no use is made of the primary vertex, and all quantities of interest are evaluated in the transverse plane.

With this selection, a yield of approximately 327 000 signal events can be expected within 30 fb^{-1} of data, with a background of 108 500 events. The efficiencies for the different criteria, which include the respective reconstruction efficiencies, are given in Table 5.3 for the signal and the different background samples, and the expected cross sections are given in Table 5.4. These do not include a requirement on the four-track invariant mass of the candidates, since the sidebands will be used later in the analysis. However, only a small fraction of these events are directly under the B_s^0 peak, and even a simple cut will reduce the number of background events by a significant factor.

5.1.5 The maximum likelihood analysis

The final state of the decay of a pseudo-scalar B meson into two vector mesons $B \to V_1 V_2$ is an admixture of CP-even and CP-odd states [130, 131, 136]. The CP-odd states correspond to transitions in which the relative orbital momentum L between the two vector mesons is

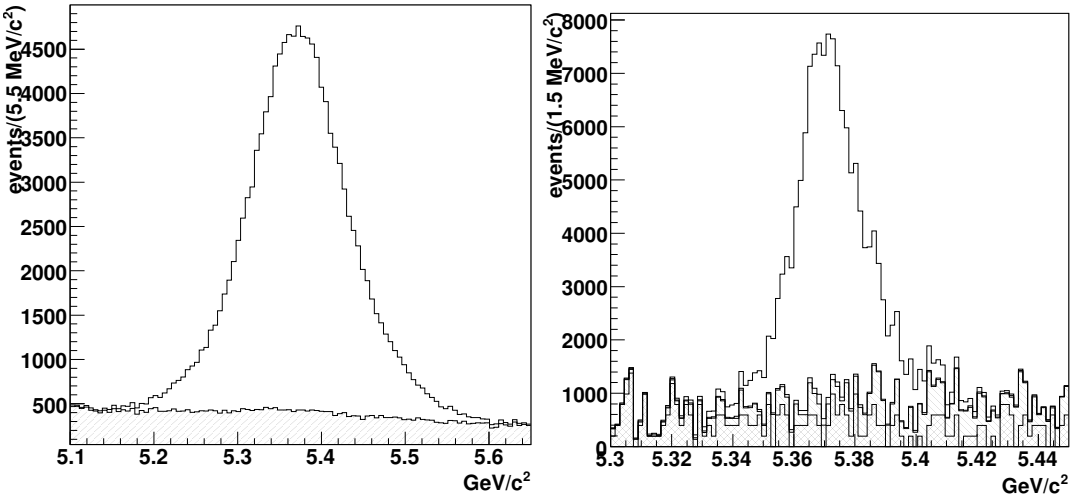

Figure 5.1: Four-track invariant mass distribution after the HLT (left) and offline (right) requirements. The right distribution includes only combinatorial background and the left distribution the expected inclusive $b \to J/\psi X$ and $B^0 \to J/\psi\, K^{*0}$ background.

1 and the CP-even states to transitions in which L is either 0 or 2. The amplitude of the decay can be decomposed in three independent decay amplitudes which correspond to the linear polarisation states of the two mesons. The first, A_0, describes states in which the linear polarisation vectors are longitudinal and is CP-even. The other two describe states in which the linear polarisation vectors are transverse, either parallel ($A_\parallel$– CP-even) or perpendicular ($A_\perp$– CP-odd) to each other.

The differential decay rate can be written as:

$$\frac{\mathrm{d}^4\Gamma(B_s(t))}{\mathrm{d}\Theta\,\mathrm{d}t} \;=\; f(\Theta,\alpha,t) \;=\; \sum_{i=1}^{6} O_i(\alpha,t)\cdot g_i(\Theta)\;, \tag{5.1}$$

where O_i are the kinematics-independent observables and g_i the angular distributions. The set of physical parameters are represented by α and the angles which define the kinematics are generically denoted Θ. The time evolution of the different observables is given by bilinear combinations of the polarisation amplitudes, $|A_0(t)|^2$, $|A_\parallel(t)|^2$, $|A_\perp(t)|^2$, $\Im(A^*_\parallel(t)A_\perp(t))$, $\Re(A^*_0(t)A_\parallel(t))$ and $\Im(A^*_0(t)A_\perp(t))$. These are functions of the widths of the two light and heavy eigenstates, Γ_L and Γ_H, the weak phase ϕ_{CKM}, the magnitudes of the amplitudes at $t = 0$ ($A_0(0)$, $A_\parallel(0)$ and $A_\perp(0)$) which describe all hadronisation effects, and, for a flavour-tagged sample, the mass difference $\Delta m_s = m_H - m_L$. Since the overall phase of the polarisation states is not observable, two strong phases are defined as $\delta_1 \equiv \arg|A^*_\parallel A_\perp|$ and $\delta_2 \equiv \arg|A^*_0 A_\perp|$. These are CP conserving, and are expected to be 0 (mod π) in the absence of final-state interactions. Assuming $SU(3)$ flavour-symmetry, the magnitudes and the two strong phases are equal for the decays $B^0_s \to J/\psi\,\phi$ and $B^0 \to J/\psi\, K^{*0}$ in unmixed samples. The measurement of these parameters is of interest to study and improve the phenomenological models used to calculate all hadronic effects.

In such decays, the kinematics are uniquely defined by a set of three angles. The transversity base is used in this analysis, in which the set of variables is $\Theta = (\cos\theta, \phi, \cos\varphi)$. In this base, (θ, φ) are the polar and azimuthal angles of the momentum of the μ^+ in the J/ψ rest frame. This coordinate system is defined such that the ϕ moves in the positive x direction and the z

axis is perpendicular to the decay plane of the decay $\phi \to K^+K^-$. The angle ψ is defined in the rest frame of the ϕ as the negative cosine of the angle between the K^+ direction and the J/ψ direction.

In order to measure the values of the different parameters, an unbinned maximum likelihood fit is performed on the observed time evolution of the angular distribution. In the absence of background and without distortion, the p.d.f. describing the data would be the original differential decay rate $f(\Theta, \alpha, t)$ (Eq. 5.1). The distortion of this distribution by the detector acceptance, trigger efficiency and the different selection criteria is taken into account by an efficiency term $\epsilon(t, \Theta)$. In addition, a term describing the background has to be added.

It is assumed that the efficiency can be factorised in two functions, the first modelling the effects of the decay length requirements and the second the distortion of the angular distribution,

$$\epsilon(t, \Theta) \;=\; \epsilon(t) \cdot \epsilon(\Theta) \; . \tag{5.2}$$

The angular efficiency is described by an expansion of products of spherical harmonics [137]:

$$\epsilon(\Theta) \;=\; \sum_{LRM} T^{\epsilon}_{LRM} \cdot \mathcal{Y}_{LRM}(\Theta) \; , \tag{5.3}$$

$$\text{with} \quad \mathcal{Y}_{LRM}(\Theta) \;=\; \sqrt{2\pi} \cdot Y_{LM}(\theta, \varphi) \cdot Y_{RM}(\psi, 0) \; , \tag{5.4}$$

where $\mathcal{Y}_{LRM}$ are orthonormal basis functions and $Y_{LM},\ Y_{RM}$ are spherical harmonic functions. In principle, L and R run from 0 to infinity and the sum over M from $-\min(L;R)$ to $+\min(L;R)$, but it has been found that the expansion can be limited to $L, R \leq 8$. These $\mathcal{Y}_{LRM}$ functions describe the partial waves involved in a scalar $\to$ vector decay [138]. The moments of the efficiency are determined from a Monte Carlo simulation with full detector simulation:

$$T^{\epsilon}_{LRM} \;=\; \int \epsilon(\Theta) \cdot \mathcal{Y}^{*}_{LRM}(\Theta) \mathrm{d}\Theta \tag{5.5}$$

$$\approx \; \frac{1}{N_{gen}} \sum_{i=1}^{N_{obs}} \frac{1}{f(\Theta_i)} \mathcal{Y}^{*}_{LRM}(\Theta_i) \; . \tag{5.6}$$

where $f(\Theta_i)$ is the expected time-integrated angular distribution (Eq. 5.1).

The time-dependent efficiency describes mainly the effects of the requirements on the proper decay length distribution. After the initial turn-on and a stable plateau, a deficit of events can be observed. Initial studies attribute this decrease in efficiency to the restrictions imposed on the seeds by the tracking regions in the HLT, which cause an additional track reconstruction inefficiency for displaced tracks such as those originating from B decays. The tolerance on the transverse and the longitudinal direction imposed on the tracking regions in the HLT results in an implicit cut on the impact parameters. Further studies are needed to find solutions to alleviate this inefficiency. Without corrections, the main effect of this inefficiency would be to lower the estimated lifetime of the longer-lived eigenstate B^H_s.

The different features in this distribution cannot easily be described by a simple function. Two sigmoidal functions combined with a quadratic function are used to describe the efficiency:

$$\epsilon(t) = \begin{cases} c \cdot \left(1 + \tanh\left(\frac{t-t_0}{\Delta t_1}\right)\right) & t < t_0 \\ (a \cdot t^2 + b \cdot t + c) \cdot \left(1 + \tanh\left(\frac{t-t_0}{\Delta t_2}\right)\right) & t > t_0 \end{cases} \; . \tag{5.7}$$

The parameters are found by fitting this function to the distribution obtained by the full Monte Carlo simulation.

The best way to gauge our ability to account for all effects and our capacity to correct them through this time-dependent efficiency curve is by comparing the proper time distributions foreseen by the simulation and observed in the data for the different B mesons. The first obvious choice is again the decay $B^0 \to J/\psi\, K^{*0}$, which is very similar to the studied B_s^0 decay, and for which the lifetime has been measured with a high precision. Any discrepancy between the efficiency determined by Monte Carlo and the data will be reflected in a mismeasurement of the B^0 lifetime. Further studies would be needed to determine the sensitivity of the efficiency on the lifetime of the selected B meson. It is dubious whether the number of B_s^0 events recovered in other trigger streams such as the dimuon stream, which has no decay length requirement, would be enough to estimate the time-dependent efficiency.

The background can be divided in two different types of distributions. The first type arises from misidentified $B^0 \to J/\psi\, K^{*0} \to \mu^+\mu^- K^+\pi^-$ events, which has a similar differential decay rate [130, 131] to the decay of interest. The width difference of the two eigenstates of the B^0 are assumed to be negligible, and no CP violation is present since the final state is flavour specific. To describe this background in the dataset, it is not possible to use its time dependent angular distribution, which is in principle well known, since all variables are mismeasured because of the misidentification of the π. In addition, the distortion of the distribution due to the various requirements is much more severe than in the case of the B_s^0. Indeed, due to its lower mass, the momentum of the π in the laboratory frame is lower than that of the corresponding K when the π is emitted in the direction opposite to the momentum of the K^{*0}.

The same set of functions $\mathcal{Y}_{LRM}(\Theta)$ (Eq. 5.4) is used to model the angular distribution $f_d(\Theta)$ of this background, with the moments computed in the following way:

$$T^b_{LRM} = \int b(\Theta)\cdot \mathcal{Y}^*_{LRM}(\Theta)\mathrm{d}\Theta \tag{5.8}$$

$$\approx \frac{1}{N_b}\sum_{i=1}^{N_b} \mathcal{Y}^*_{LRM}(\Theta_i)\ , \tag{5.9}$$

Here as well, the expansion is done up to $L, R \leq 8$. The functions are obtained by a Monte Carlo simulation and can be cross-checked by a fully reconstructed sample of well-identified $B^0 \to J/\psi\, K^{*0}$ decays misreconstructed as B_s^0 candidates.

The time dependence of this background is modelled as a single exponential decay, again with a time-dependent efficiency. The lifetime τ_d is left as a free parameter, since the mismeasurement of the proper decay length precludes using the well-measured lifetime of the B^0.

The other sources of background are assumed to have no angular dependence. The distribution of their proper decay time is modelled by two exponential decays, the first describing the short-lived prompt background and the second misidentified long-lived heavy-flavour hadrons.

A better separation of the signal and background is obtained by using the events in a wider invariant mass region between 5.219 and $5.559\,\mathrm{GeV/c^2}$, and including in the fit the distribution of the invariant mass of the candidates. The distribution of the B_s^0 candidates is modelled by a Gaussian $G_s(m; m_s, \sigma_s)$, where m_s is the mass of the B_s^0 meson and σ_s the variance

due to the reconstruction. The distribution of the misidentified $B^0 \to J/\psi\, K^{*0}$ decays can reasonably well be modelled in the chosen region by a Gaussian $G_d(m; m_d, \sigma_d)$. Because of the misidentification of the pion, m_d will not correspond to the true mass of the B^0 meson, and will be left as a free parameter in the fit. The other sources of background are assumed to have a flat mass distribution and will be modelled by a linear function $L(m)$.

The total p.d.f. to be fit is thus given by

$$\begin{aligned} \mathcal{P} &= (1 - b_d - b_c) \cdot \epsilon(t, \Theta) \cdot f(\Theta, \alpha, t) \cdot G_s(m; m_s, \sigma_s) \\ &\quad + b_d \cdot f_d(\Theta) \cdot \epsilon(t) \cdot \frac{1}{\tau_d} e^{-t/\tau_d} \cdot G_d(m; m_d, \sigma_d) \\ &\quad + b_c \cdot \epsilon(t) \cdot \left(\frac{1}{\tau_{cl}} e^{-t/\tau_{cs}} + \frac{1}{\tau_{cl}} e^{-t/\tau_{cl}} \right) \cdot L(m) \ , \end{aligned} \tag{5.10}$$

where b_d, respectively b_c, are the fraction of misidentified B^0 background, respectively combinatorial background in the sample. These parameters are left free in the fit. The resolution of the proper decay length is taken into account by convolving the p.d.f. with a Gaussian resolution function. The standard deviation of the Gaussian is taken as the uncertainty of each candidate's proper decay length measurement multiplied by a scale factor, which is left free in the fit. Since the uncertainties of the measured angles are found to be small, these are not taken into account in the fit. A contribution is added to the systematic uncertainty to reflect this omission.

5.1.6 Result

Due to the high production cross sections of the identified backgrounds, only limited samples could be generated and analysed, which do not permit to have a final dataset with the foreseen signal-to-background ratio. Indeed, the signal sample corresponds to an integrated luminosity of $6.8\,\text{fb}^{-1}$, while the inclusive background corresponds to an integrated luminosity of barely $48\,\text{pb}^{-1}$. The situation is somewhat better for the decay $B^0 \to J/\psi\, K^{*0}$, for which the sample corresponds to an integrated luminosity of $1.3\,\text{fb}^{-1}$.

First, a fit was performed on the complete set of selected and associated B_s^0 candidates only, using the efficiency functions determined in the previous section. The relative width difference $\Delta\Gamma_s/\bar{\Gamma}_s$ can be determined with an uncertainty of 0.016 (Table 5.5), but no sensitivity on the weak phase and the strong phases is obtained.

Table 5.5: Results of the maximum likelihood fit for 73813 signal events.

Parameter	Input value	Result	Stat.error	Rel.error
$\lvert A_0(0)\rvert^2$	0.57	0.57398	0.00267	0.4%
$\lvert A_{\lvert\rvert}(0)\rvert^2$	0.217	0.21808	0.00473	2.1%
$\lvert A_\perp(0)\rvert^2$	0.213	0.20794	0.00396	1.9%
$\bar{\Gamma}_s$	0.712ps^{-1}	0.712358ps^{-1}	0.00350643ps^{-1}	0.5%
$\Delta\Gamma_s$	0.142ps^{-1}	0.134645 ps^{-1}	0.0108247ps^{-1}	8.0%
$\Delta\Gamma_s/\bar{\Gamma}_s$	0.2	0.189013	0.0157993	8.4%
δ_1	π	2.94405	0. 632682	
δ_2	0	-0.109493	0.639713	
ϕ_{CKM}	-0.04	-0.0297427	0.0758856	

Then, a sample corresponding to an integrated luminosity of $1.3\,\text{fb}^{-1}$ is considered, which allows to have a realistic ratio of $B^0 \to J/\psi\, K^{*0}$ and signal events. With the low number of background events which remain after all selection requirements, an accurate model through the described p.d.f. is not possible. In addition, the low number of $B^0 \to J/\psi\, K^{*0}$ events does not permit an accurate estimate of either the angular distribution or of its time-dependent efficiency. As such, the background events are simply added to the dataset and their expected distribution is not included in the p.d.f. used in the fit. The p.d.f. would thus simply describe the B_s^0 distribution:

$$\mathcal{P} = \epsilon(t, \Theta) \cdot f(\Theta, \alpha, t)$$

With such a fit in which the invariant mass of the candidates is not taken into account, a requirement on the invariant mass of the candidates would obviously be made, choosing a window of $\pm 36\,\text{MeV/c}^2$ around the world-average B_s^0 mass. This reduces the number of B^0 background events by a further 59%, while reducing the number of signal candidates by 2.9%. The results of the fit without background is given in Table 5.6 and with background in Table 5.7. With the lower number of B_s^0 candidates, the statistical uncertainty of the measurement is, as expected, markedly worse. As can be seen, the influence of the background is very small, with only a slight degradation of the width difference. The distribution of the proper decay length of the selected events with the fit projection is shown in Figure 5.2.

Table 5.6: Results of the maximum likelihood fit for an integrated luminosity of $1.3\,\text{fb}^{-1}$ (signal only).

Parameter	Input value	Result	Stat.error	Rel.error
$\lvert A_0(0)\rvert^2$	0.57	0.5859	0.0062	1.1%
$\lvert A_{\lvert\lvert}(0)\rvert^2$	0.217	0.2141	0.0078	3.6%
$\lvert A_\perp(0)\rvert^2$	0.213	0.2002	0.0064	3.2%
$\bar{\Gamma}_s$	0.712ps^{-1}	0.7018ps^{-1}	0.0081ps^{-1}	1.2%
$\Delta\Gamma_s$	0.142ps^{-1}	0.1470ps^{-1}	0.0256ps^{-1}	17.4%
$\Delta\Gamma_s/\bar{\Gamma}_s$	0.2	0.2095	0.0371	18.1%

Table 5.7: Results of the maximum likelihood fit for an integrated luminosity of $1.3\,\text{fb}^{-1}$ (signal and background).

Parameter	Input value	Result	Stat.error	Rel.error
$\lvert A_0(0)\rvert^2$	0.57	0.5823	0.0061	1.1%
$\lvert A_{\lvert\lvert}(0)\rvert^2$	0.217	0.2130	0.0077	3.6%
$\lvert A_\perp(0)\rvert^2$	0.213	0.2047	0.0065	3.2%
$\bar{\Gamma}_s$	0.712ps^{-1}	0.7060ps^{-1}	0.0080ps^{-1}	1.1%
$\Delta\Gamma_s$	0.142ps^{-1}	0.1437 ps^{-1}	0.0255ps^{-1}	17.7%
$\Delta\Gamma_s/\bar{\Gamma}_s$	0.2	0.2036	0.0374	18.4%

5.1.7 Systematics and detector effects

The list of systematic uncertainties which were considered are summarised in two tables. The first, Table 5.8, summarises the uncertainties which affect the HLT rate and the number of foreseen events after all selection requirements. The second, Table 5.9, summarises the uncertainties which affect the measurement of the various parameters.

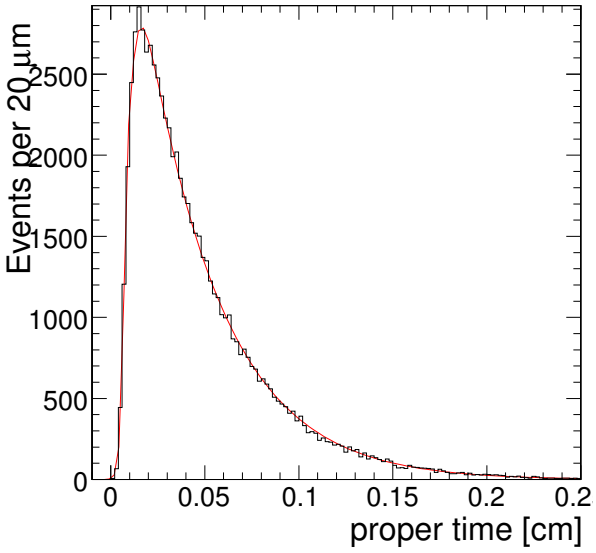

Figure 5.2: Distributions of the proper decay length of the selected signal and background events with fit projection.

- Signal and background statistics:
  Among the various uncertainties listed in Section 5.1.2, the largest single source of uncertainty in the estimate of the number of events is obviously the poor knowledge of the $B_s^0 \to J/\psi\,\phi$ branching ratio. The uncertainties quoted on the estimates above do not include the uncertainties on the total $b\bar{b}$ cross section at LHC energies, the $b \to B^0$ fragmentation functions, the transverse momentum distribution of b quarks. However, since both the signal and background are proportional to the same $b\bar{b}$ cross section, the signal-to-background ratio is unaffected by the corresponding uncertainty.
- Track reconstruction efficiency:
  A 1% uncertainty per track on the track reconstruction efficiency is assumed for all tracks.
- Muon reconstruction:
  The selection relies heavily on the correct identification of muons. A 1% uncertainty per track on the combined muon identification procedure is assumed.
- Tracker and muon detector misalignment:
  The study has been conducted with a perfectly aligned detector. To gauge the sensitivity of the analysis with respect to the alignment the analysis has been repeated on a detector with the short-term alignment scenario. This scenario is expected to be representative of the relative misalignment of the detector components during the initial data taking period [85] The effects of misalignment of the tracker on various aspects of track and vertex reconstruction have been extensively studied and reported in [139, 140]. The degradation affect both the selection, mostly through the requirement on the significance of the transverse decay length of the J/ψ in the HLT, and the analysis, through the degradation of the measurement of the proper decay length. The resolution of the latter is degraded from 24 μm for a perfectly aligned detector to 32 μm with the short-term alignment. The HLT efficiency is degraded by some 17% with respect to a perfectly aligned detector.

Table 5.8: List of systematic uncertainties with effect on the predictions of the rates.

Source	HLT uncert.	Offline uncert.	Common uncert.
Branching ratio B_s^0			36.4 %
Branching ratio B^0			6 %
Branching ratio $b \to J/\psi X$			9 %
Tracking inefficiency	2 %	2%	
Muon reconstruction	-	1.4%	
Misalignment	17%	-	

- Background distributions:
  To gauge the influence of the background on the fit, the variation observed between the fits performed on the reduced $1.3\,\text{fb}^{-1}$ dataset with and without these events is added to the systematic uncertainty ("Bckg. distrib." in the table).

  Since the signal-to-background ratio has a significant uncertainty, the fit performed on the reduced $1.3\,\text{fb}^{-1}$ sample is repeated varying the number of B_s^0 signal events to match the uncertainty in the signal-to-background ratio. For this estimate, a different uncertainty for the B_s^0 branching fraction has been chosen, since it is believed that it will be measured again in the current run of the Tevatron. Two main uncertainties plagued the measurement done at CDF in Run I, the low number of observed B_s^0 candidates and the uncertainty on the fragmentation. Based on recent publications, it is estimated that approximately 30 times more $B_s^0 \to J/\psi\,\phi$ decays than in Run 1 should already be collected in the current dataset of $1\,\text{fb}^{-1}$. The uncertainty of the branching fraction is therefore reduced to 20%. For the other uncertainties, the numbers listed in Table 5.8 are used. The variation observed on the fit is listed under the heading "S/B ratio". In a larger dataset, where the full p.d.f. (Eq. 5.11) is used, the influence of the uncertainty on the signal-to-background ratio should be much smaller, since the fractions of background events in the dataset are free parameters in the fit.
- Distortion of the proper-time distribution ("$c\tau$ distortion"):
  Other fits were then performed where the parameters of the time dependent efficiency function are varied by one standard deviation. The mean variation of the fitted parameters was added to the systematic uncertainty. As already mentioned, the decay $B^0 \to J/\psi\,K^{*0}$ can be used to compare the accuracy of this model by comparing the Monte Carlo prediction with the efficiency function observed in the data.
- Distortion of the angular distributions ("Ang. distortion"):
  The expansion used to model the distortion of the angular distributions (Eq. 5.3) is limited to $L, R \leq 8$. When limiting the expansion to $L, R \leq 6$ or $L, R \leq 10$, the result of the fit shows negligible differences. In addition, to account for the possibility that the efficiencies do not factorise and that the angular efficiency is grossly miscalculated, the fit is also repeated without the angular efficiency, i.e. without correction of the distortion. While this has little influence on the estimated lifetimes, a large variation is found for the amplitudes. This variation is used as systematic uncertainty.
- Resolution on the angular variables ("Resolution"):
  In order to estimate the influence of the uncertainties of the angles and the proper decay length on the fit, a fully controlled toy Monte Carlo was used, in which only

Table 5.9: List of systematic uncertainties with effect on the measurements.

Source	$\|A_0(0)\|^2$	$\|A_{\|\|}(0)\|^2$	$\|A_\perp(0)\|^2$	$\bar{\Gamma}_s$	$\Delta\Gamma_s/\bar{\Gamma}_s$
Bckg. distrib.	0.0034	0.0011	0.0045	0.0043	0.0059
S/B ratio	0.0037	0.0001	0.0024	0.0025	0.0055
Resolution	-	-	-	0.00060	0.0045
Ang. distortion	0.0143	0.0061	0.0082	0.00083	0.0010
$c\tau$ distortion	0.0016	0.00073	0.0023	0.0221	0.0146
Alignment	0.00012	0.00042	0.00055	0.00040	0.0014
Total	0.0152	0.0063	0.0099	0.0227	0.0173

the proper time and angles were generated according to the expected p.d.f. and smeared with Gaussian resolution functions. The default standard deviations are taken to be equal to those measured in the Monte Carlo with full detector simulation. The simulation was then repeated without smearing and with a substantial smearing, where the resolution is taken to be two times larger than in the default simulation. The value of parameters found in both cases were very close to the values found with the default smearing, and the observed variation is added to the systematic uncertainty.

5.1.8 Conclusion

The present section describes a study on the selection of the $B_s^0 \to J/\psi\,\phi$ decay and the measurement of the width difference $\Delta\Gamma_s$ in absence of flavour tagging. An example of a trigger algorithm is presented which would be efficient for this decay and would reject a large fraction of the background. It is based on the identification of J/ψ and B_s^0 candidates with a displaced decay vertex. Nevertheless, this trigger precludes the selection of other decays of the B meson, and should certainly evolve as a true precursor to a B physics trigger. Indeed, the strategy proposed for the Level-2 would select inclusive $b \to J/\psi$ decays with high efficiency and good purity with respect to the prompt J/ψ background. Large uncertainties nevertheless plague the estimates of rates, since large uncertainties remain on the b-quark and prompt J/ψ production cross sections, on their momentum distributions, and on the $b \to B_s^0$ fragmentation function.

A first measurement of one of the main parameters of the B_s^0 system, the relative difference of the widths of the weak eigenstates could be determined with a statistical uncertainty of 0.011 in a sample corresponding to an integrated luminosity of $10\,\text{fb}^{-1}$. A first measurement undertaken on approximately $1.3\,\text{fb}^{-1}$ of data could already yield a measurement with an uncertainty of 20% (Table 5.10). A natural extension of this study should be a tagged analysis, for which flavour tagging algorithms need to be developed.

5.2 Associated production of MSSM heavy neutral Higgs bosons $\mathrm{b\bar{b}H(A)}$ with $\mathrm{H(A)} \to \tau\tau$

5.2.1 Introduction

The observation of a heavy neutral scalar accompanied by b-jets and decaying into two τ leptons would be an important sign of a MSSM Higgs sector. In the MSSM the associated Higgs boson production $\mathrm{gg} \to \mathrm{b\bar{b}H(A)}$ is dominant at large values of $\tan\beta$. The cross section of the $\mathrm{gg} \to \mathrm{b\bar{b}H(A)}$, $\mathrm{H(A)} \to \tau\tau$ process is proportional to $\tan^2\beta_{\text{eff}}$ and will be used in

Table 5.10: Results of the maximum likelihood fit for an integrated luminosity of $1.3\,\mathrm{fb}^{-1}$ (signal and background).

Parameter	Input value	Result	Stat. error	Sys. error	Total error	Rel. error
$\lvert A_0(0)\rvert^2$	0.57	0.5823	0.0061	0.0152	0.0163	2.8%
$\lvert A_{\lvert\lvert}(0)\rvert^2$	0.217	0.2130	0.0077	0.0063	0.0099	4.6%
$\lvert A_{\perp}(0)\rvert^2$	0.213	0.2047	0.0065	0.0099	0.0118	5.8%
$\bar{\Gamma}_s$	0.712ps^{-1}	0.7060ps^{-1}	0.0080ps^{-1}	0.0227ps^{-1}	0.0240ps^{-1}	3.4%
$\Delta\Gamma_s$	0.142ps^{-1}	0.1437 ps^{-1}	0.0255ps^{-1}	0.0113ps^{-1}	0.0279ps^{-1}ps^{-1}	19%
$\Delta\Gamma_s/\bar{\Gamma}_s$	0.2	0.2036	0.0374	0.0173	0.0412	20%

a global fit together with other relevant measurements to determine the SUSY parameters simultaneously.

This channel is an excellent benchmark for the b- and τ-tagging, jet and missing $\mathrm{E_T}$ reconstruction. The final state with two τ-jets requires τ tagging both at Level-1 and High Level trigger. Along with reconstruction and tagging issues, a large number of various Standard Model backgrounds including QCD multi-jet production must be well understood from the real data to be able to establish a discovery.

5.2.2 Event generation

The signal events were generated by PYTHIA using processes the 181 ($\mathrm{gg} \to \mathrm{b\bar{b}H}$) and 152 ($\mathrm{gg} \to \mathrm{H}$) for three values of the Higgs boson mass: 200, 500 and 800 GeV/c^2. The backgrounds considered were QCD multi-jet events (for $\tau\tau \to$ jj mode), $\mathrm{t\bar{t}}$, $\mathrm{b\bar{b}}$, Drell-Yan production of Z/γ^*, W+jet, Wt and $\tau\tau\mathrm{b\bar{b}}$. All background processes except $\tau\tau\mathrm{b\bar{b}}$ were generated with PYTHIA. The $\tau\tau\mathrm{b\bar{b}}$ process was generated by COMPHEP.

In order to reduce CPU time for full detector simulation and event reconstruction loose preselections were applied for some of the backgrounds at the generation level. The description of the pre-selections for each final state can be found in the following sections.

The cross sections for the associated Higgs boson production $\mathrm{gg} \to \mathrm{b\bar{b}H(A)}$ and the branching ratio $\mathrm{H(A)} \to \tau\tau$ were calculated using FeynHiggs2.3.2 [141–143] [1] in the $\mathrm{m_h^{max}}$ scenario with μ=200 GeV/c^2 (see Section 11.3.1).

The uncertainty of the measured cross section of the $\mathrm{b(\bar{b})A}, \mathrm{A} \to \tau\tau$ process will include the uncertainty of the Monte Carlo generation. The verification of the Monte Carlo generation for the Higgs boson production with the associated b-jets will be done with the real data using $\mathrm{b\bar{b}Z}$ ($\mathrm{Z} \to \ell\ell$) events [144].

5.2.3 Level-1 and High Level trigger selections

The $\tau\tau \to$ jj final state is triggered by Level-1 single or double tau triggers with thresholds of 93 GeV for the single and 66 GeV for the double tau trigger. It is followed by the double τ-jet tagging at High Level trigger. Currently there are two selection strategies at HLT under consideration [145]. In the first strategy the calorimeter isolation using the electromagnetic calorimeter is applied to the first τ-jet in order to reduce the Level-1 output rate by a factor

[1] the code can be obtained from `http://www.feynhiggs.de`

of 3. The tracker isolation is then applied on both jets using the tracks reconstructed with the pixel detector only. The second strategy performs tracker isolation right after the Level-1 trigger decision and uses the full tracker with regional track finding and a restricted number of hits to reconstruct tracks. In this analysis the first method is exploited.

The $\tau\tau \rightarrow \mu$j final state uses the single muon trigger at Level-1 with a threshold of 14 GeV. At the High Level the combined muon-plus-τ-jet trigger is used with thresholds of 15 GeV for the muon and of 40 GeV for the τ-jet.

The $\tau\tau \rightarrow$ ej final state uses the Level-1 single electron trigger with a threshold of 23 GeV together with the combined electron-plus-τ-jet trigger with thresholds of 14 GeV for the electron and 52 GeV for the τ-jet. At High Level again the single electron trigger with a threshold of 26 GeV and the combined electron-plus-τ-jet trigger with a threshold of 16 GeV for the electron is used. No threshold is applied for the τ-jet candidate.

At High Level trigger, for both the $\tau\tau \rightarrow \mu$j and the $\tau\tau \rightarrow$ ej final states, the ECAL and pixel track isolation is applied on the τ-jet candidate similar to what is used in the double τ-jet trigger. For the lepton (e and μ) the same selections are used as for the single electron and muon High Level triggers. The lepton and τ-jet are required to stem from the same vertex found with the pixel detector. Only the tracks from this vertex are used in the tracker isolation.

The search strategy for τ-jet candidates at High Level trigger for the combined muon-plus-τ-jet and electron-plus-τ-jet triggers is the following: Two calorimeter jets are always reconstructed with the regional jet finder in the regions given by the two highest $\mathrm{E_T}$ Level-1 τ-jets. For the muon-plus-τ-jet trigger the first (highest $\mathrm{E_T}$) jet is taken as τ-jet candidate. For the electron-plus-τ-jet trigger the requirement of non collinearity of the jet and the HLT electron candidate, $\Delta\mathrm{R(e-jet)}$ >0.3, is checked for each jet, where $\Delta\mathrm{R(e-jet)}$ is the distance in η-φ space between the electron and the jet. The first non collinear jet is taken as the τ-jet candidate.

5.2.4 Off-line event selection

The first step in the off-line analysis is the τ-jet identification. The calorimeter jet is reconstructed in the η-φ region of the High Level trigger τ-jet candidate with the iterative cone algorithm using a cone size of 0.4. A number of requirements for τ-jet identification [145] is applied in addition to the tracker isolation which is tighter off-line than at the HLT and uses the tracks reconstructed with the full tracker. The additional τ-jet identification criteria include requirements to have one or three tracks in the signal cone and opposite charge of the two τ-jets for the $\tau\tau \rightarrow$ jj mode or the lepton and the τ-jet for the $\tau\tau \rightarrow \ell$j modes and cuts on the transverse impact parameter and on the p_T of the leading track in the signal cone. Finally an electron rejection criterion was applied for the jets. The τ-jet tagging reduces the QCD multi-jet (including $\mathrm{b\bar{b}}$) and the W+jet backgrounds.

The associated $\mathrm{b\bar{b}H(A)}$ production dominates at high values of $\tan\beta$, thus it is natural to apply b-jet tagging which must suppress Drell-Yan $\tau\tau$ production and eliminate further the QCD multi-jet and the W+jet backgrounds. Since the b-jets in the signal are very soft in $\mathrm{E_T}$ and have flat distribution in pseudorapidity only single b tagging is applied. Furthermore, it is possible to veto events with additional jets to reduce $\mathrm{t\bar{t}}$ background. The τ-jets found in the first step are not considered for b tagging. Non τ-jet candidates are reconstructed with the iterative cone algorithm using a cone size of 0.5.

The energy of the τ-jet is corrected with a dedicated calibration obtained from Monte-Carlo sample of single τ-jets at low luminosity. The energy of other jets in the event is corrected applying Monte Carlo calibration evaluated from the QCD multi-jet events at low luminosity.

5.2.5 Method of the Higgs boson mass reconstruction

Despite the escaping neutrinos, the Higgs boson mass can be reconstructed in the $\mathrm{H} \to \tau\tau$ channels from the visible τ momenta (leptons or τ-jets) and the missing transverse energy ($\mathrm{E_T^{miss}}$) with the collinearity approximation for the neutrinos from highly boosted τ's. The mass resolution depends on the angle $\Delta\varphi$ between the visible τ momenta as $1/\sin(\Delta\varphi)$ and is sensitive to the $\mathrm{E_T^{miss}}$ measurement, both in magnitude and particularly in direction. The measurement of $\mathrm{E_T^{miss}}$ is affected by the non-linear calorimeter response. A method to improve the $\mathrm{E_T^{miss}}$ scale based on the jet energy corrections was used [146, 147]. The correction of the missing $\mathrm{E_T}$ scale improves the reconstruction efficiency by reducing the number of events with negative reconstructed τ lepton and neutrino energies. In particular, for the case of the $\tau\tau \to$ jj final state the efficiency is improved by factor of $\simeq 1.6$. The $\tau\tau$ mass reconstruction method will be verified with the real data using $\mathrm{Z} \to \tau\tau \to \mathrm{e}(\mu)+\mathrm{jet}$ and $\mathrm{Z} \to \tau\tau \to \mathrm{e}+\mu$ channels [144, 148].

5.2.6 $\mathrm{H} \to \tau\tau \to 2\tau + \mathrm{jet}$ analysis

A detailed description of the analysis can be found in [149].

5.2.6.1 Event generation and pre-selections

The $\mathrm{t\bar{t}}$, Drell-Yan production of Z/γ^*, W+jet and Wt backgrounds were generated with PYTHIA, forcing $\mathrm{W} \to \tau\nu$ and $\mathrm{Z}/\gamma^* \to \tau\tau$ decays. The TAUOLA package was used for τ-lepton decays into all possible decay modes.

The Z/γ^* generation was split into three bins of generated diτ-lepton mass $\mathrm{m_{\tau\tau}}$: 80-130 GeV/c^2, 130-300 GeV/c^2 and >300 GeV/c^2. The $\tau\tau\mathrm{b\bar{b}}$ generation was divided into two bins of generated diτ-lepton mass $\mathrm{m_{\tau\tau}}$: 60-100 GeV/c^2 and >100 GeV/c^2. The $\tau\tau\mathrm{b\bar{b}}$ background, generated with COMPHEP, was propagated to PYTHIA for showering, hadronisation and τ lepton decays into all possible modes.

The W+jet background was generated using PYTHIA processes 16 and 31 and with $\mathrm{\hat{p}_T}$ >65 GeV/c. The QCD multi-jet background generation was done for four bins in $\mathrm{\hat{p}_T}$: 50-80, 80-120, 120-170 and $>$ 170 GeV/c.

The loose pre-selections at the level of generation were applied for all backgrounds (except $\tau\tau\mathrm{b\bar{b}}$): the event was required to have at least two "τ-like" jets. The jets were reconstructed with the PYTHIA PYCELL routine using a cone size of 0.5. A jet is selected as "τ-like" if it has $\mathrm{E_T^{MC}}$ >50 GeV, $|\eta^{\mathrm{MC}}|$ <2.4 and a transverse momentum of the leading stable charged particle in the jet, $\mathrm{p_T^{MC}}$, >30 GeV/c. These cuts are looser than the ones applied at the trigger and off-line τ-jet selections. For Z/γ^* background no cut was applied on $\mathrm{p_T^{MC}}$.

For the signal events the Higgs boson was forced to decay into two τ leptons and the τ lepton was decayed hadronically using TAUOLA. No pre-selections were applied for the signal events.

5.2.6.2 Event selections

The calorimeter τ-jet jet candidates are reconstructed in the η-φ regions of the High Level trigger τ-jet candidates, thus no "volunteers" are searched for. This is motivated by the high ($\simeq$ 100%) purity of the HLT τ-jet candidates (fraction of true τ-jets matched with τ-jet candidates)

A cut on the uncalibrated transverse jet energy for each of the two τ-jet candidates was required. It was E_T >50 GeV for M_A=200 GeV/c^2. For higher Higgs boson masses asymmetrical cuts were used: 100, 50 GeV for M_A=500 GeV/c^2 and 150, 50 GeV for M_A=800 GeV/c^2. It allows more effective rejection of the QCD multi-jet background. The following τ-jet identification criteria were then used:

- tracker isolation with parameters: R_m=0.1, R_S=0.04, R_i=0.5, p_T^i=1 GeV/c;
- transverse momentum of the leading track >35 GeV/c;
- one or three tracks in the signal cone N_{tr}^S for M_A=200 GeV/c^2. For higher Higgs boson masses an effective background rejection is only possible by requiring only one track in the signal cone.

Finally, the two τ-jet candidates were required to have opposite charge. The charge was calculated as the sum of charges of the tracks in the signal cone.

After identification of two τ-jets the other jets in the event were considered. It was required to have only one additional jet with uncalibrated energy E_T^{raw} >20 GeV and $|\eta|$ <2.4. It had to be tagged as b-jet. The b-jet identification was performed using the impact parameter tagging in 3D space [150]. The jet had to have at least three tracks with an impact parameter significance > 2. The purity of the b-tagged jet for the signal is very high (>95%).

The diτ-jet mass reconstruction efficiency is affected by the requirements to have a positive reconstructed energy of both neutrinos, $E_T^{\nu_1,\nu_2}$ >0. In the missing E_T corrections jets with raw energy E_T^{raw} >25 were used.

5.2.6.3 Expected number of selected events

This section summarises the event selections, the corresponding cross sections and expected number of events for the signal and the background processes after the selections. The efficiency of all selections shown in the tables of this section was evaluated relative to the previous selection.

Signal

Table 5.11 summarises the expectations for a signal of M_A = 200, 500 and 800 GeV/c^2. The signal cross sections and the branching ratios were obtained for the m_h^{max} scenario with μ=200 GeV/c^2 (see Section 11.3.1).

QCD multi-jet background

Despite the huge amount of generated events (more than one million) and generation preselections, the statistics of the QCD multi-jet background events is not enough to ensure a large number of Monte Carlo events passing all the selections. In order to decrease the statistical uncertainties a factorisation of the selections was applied. All selections were combined in three groups as shown in Table 5.12. Group1 includes the Level-1 trigger and the calorimetric reconstruction of the τ-jets (at HLT and offline). It includes also the cut on the trans-

Table 5.11: The summary table of the selections for signals of M_A = 200, 500 and 800 GeV/c^2.

	m_A = 200 GeV/c^2 $\tan\beta$ = 20	m_A = 500 GeV/c^2 $\tan\beta$ = 30	m_A = 800 GeV/c^2 $\tan\beta$ = 40
Cross sections and branching ratios			
$\sigma(gg \to b\bar{b}(A+H))$ (fb)	45795+44888	2741+2744	677+677
BR($H/A \to \tau\tau$)	0.1	0.082	0.087
BR($\tau \to$ hadrons)^2	0.65$\times$ 0.65		
$\sigma\times$ BR (fb)	3831	190	49.8
Experimental selection efficiencies			
Level-1 Trigger	0.506	0.854	0.896
HLT	0.289	0.319	0.314
two off-line calo τ jets	0.997	0.999	0.999
cuts on E_T τ jets	0.430	0.755	0.780
two off-line τ candidates	0.674	0.716	0.675
$p_T^{ltr} > 35$ GeV/c	0.326	0.616	0.713
tracker isolation	0.859	0.950	0.954
N_{tracks} in signal cone	0.81	0.67	0.78
$Q_{\tau 1}\times Q_{\tau 2}$ = -1	0.98	0.94	0.94
$\geq$ 1 extra jet, $E_T^{raw} > 20$ GeV, $\lvert\eta\rvert$ <2.4	0.21	0.27	0.31
only 1 extra jet, $E_T^{raw} > 20$ GeV, $\lvert\eta\rvert$ <2.4	0.83	0.82	0.78
$M_{\tau\tau}$ reconstruction efficiency			
$E_{\tau 1,\tau 2} > 0$	0.93	0.93	0.92
$E_{\nu 1,\nu 2} > 0$	0.56	0.67	0.67
total mass reconstruction	0.52	0.62	0.62
b tagging of the extra jet	0.36	0.44	0.41
$M_{\tau\tau}$ mass window	150-300 GeV/c^2	400-700 GeV/c^2	600-1100GeV/c^2
mass window efficiency	0.81	0.73	0.81
total efficiency	2.5×10^{-4}	2.4×10^{-3}	3.6×10^{-3}
σ after selections (fb)	0.96	0.46	0.19
number of events for 60 fb^{-1}	58.0	27.0	11.0

verse energy of the jets. After the event passed the Group1 selections the two other selection groups (Group2 and Group3) were applied independently. Group2 is essentially the τ-jet identification part of the analysis, i.e. the tracker isolation (at HLT and off-line), the cut on the p_T of the leading track and the selection on the number of tracks inside the signal cone. Group3 describes the selections on the one extra jet in the event, the b tagging and the diτ-jet mass reconstruction. The choice of the second and third selection groups was made minimising the correlation among them. A further factorisation was done for some selections inside the groups. Table 5.12 summarises the selections and the QCD multi-jet background estimates for the signal of M_A=200 GeV/c^2. The requirement to have opposite charge τ-jet candidates ($Q_1 \times Q_2$=-1) is not included in Table 5.12. It reduces the QCD multi-jet background by another factor of two, leading to 104 events of the QCD multi-jet background expected with 60 fb^{-1}. With the selections applied to search for signals of M_A=500 GeV/c^2 and M_A=800 GeV/c^2 the expected numbers of the QCD multi-jet background with 60 fb^{-1} are 25.0 and 4.0, respectively.

Irreducible background

The irreducible background which remains after all selections were applied is the small part of the total background dominated by the QCD multi-jet events. Table 5.13 summarises the expected number of events from the irreducible background with 60 fb^{-1} for the selections used to search for a signal of M_A=200 GeV/c^2. In total, 6.0 events are expected. The efficiencies of some of the selections are also shown in the table. With the selections applied to search for signals of M_A=500 GeV/c^2 and M_A=800 GeV/c^2 the expected numbers of the irreducible background with 60 fb^{-1} are 4.0 and 1.0, respectively.

5.2.6.4 Detector effects, experimental systematics and evaluation of the background from data.

E_T^{miss} and jet energy scale uncertainties

The effect of the E_T^{miss} and the jet energy scale uncertainty on the Higgs boson mass reconstruction efficiency was estimated. The E_T^{miss} is reconstructed with the Type 1 corrections in the following form:

$$E_{Tx(y)}^{miss} = -(E_{Tx(y)}^{raw} + \sum_{jets}(E_{Tx(y)}^{corr.jet} - E_{Tx(y)}^{rawjet})) \quad (5.11)$$

where $E_{Tx(y)}^{raw}$ is the sum over the raw calorimeter tower energies from calorimeter towers and the jet sum in the equation is over jets with a reconstructed E_T^{raw} >25 GeV. The formula can be rewritten in the form:

$$E_{Tx(y)}^{miss} = -([E_{Tx(y)}^{raw} - \sum_{jets} E_{Tx(y)}^{rawjet}]_{low\ E_T} + [\sum_{jets} E_{Tx(y)}^{corr.jet}]_{high\ E_T}) \quad (5.12)$$

representing of low and high E_T parts. For the low E_T part a scale uncertainty of 10% was applied, while for the high E_T part 3% uncertainty was used. The variation of the scale is applied independently for the two parts to obtain the maximal upper and lower deviations from the case with no uncertainty. It was found that the E_T^{miss} scale uncertainty brings the largest contribution to the uncertainty of the Higgs boson mass reconstruction efficiency. In the worst case the uncertainty reaches 3%. The mean fitted value of the $M_{\tau\tau}$ distribution for a signal of M_A=500 GeV/c^2 is varied from -10 GeV/c^2 to +16 GeV/c^2 relative to the mean value evaluated without the scale uncertainty taken into account.

Table 5.12: The summary table of the selections for the QCD multi-jet background. The selections are factorised as explained in the text. The requirement to have opposite charge τ-jet candidates ($Q_1 \times Q_2$=-1) is not included.

	QCD dijet background in bins of generated $\hat{p}_T$			
	>170 GeV/c	120-170 GeV/c	80-120 GeV/c	50-80 GeV/c
σ (fb)	1.33×10^{8}	5.03×10^{8}	2.94×10^{9}	2.08×10^{10}
$\varepsilon_{\text{kine pres.}}$	2.12×10^{-1}	4.19×10^{-2}	5.77×10^{-3}	2.44×10^{-4}
Group1 cuts: Level-1 trigger + L2 and offline calo reco + E_T cut				
Level-1 trigger	0.562	0.726	0.715	0.461
two Level 2 calo jets with $\Delta R_{J\,J} > 1.0$	0.927	0.959	0.982	0.987
two off-line calo τ jets	0.975	0.975	0.982	0.994
cuts on E_T τ jets	0.753	0.804	0.774	0.343
$\varepsilon_{\text{Group1}}$	0.383	0.547	0.534	0.155
Group2 cuts: τ-jet identification at HLT and off-line				
HLT Calo+Pxl τ trigger	7.15×10^{-4}	1.81×10^{-3}	4.44×10^{-3}	1.12×10^{-2}
two off-line τ candidates	0.86	0.84	0.825	0.84
$p_T^{ltr} > 35$ GeV/c	0.47	0.41	0.42	0.38
tracker isolation	0.24	0.21	0.25	0.35
Factorised inside group 2				
1 or 3 prongs in 1st τ jet	0.66	0.92	0.63	0.72
1 or 3 prongs in 2nd τ jet	0.48	0.54	0.65	0.72
$\varepsilon_{\text{Group2}}/\varepsilon_{\text{Group1}}$	2.30×10^{-5}	6.33×10^{-5}	1.63×10^{-4}	6.54×10^{-4}
Group3 cuts: extra jet reco and b tagging plus $M_{\tau\tau}$ reco and mass window				
≥ 1 extra jet, $E_T^{raw} > 20$ GeV, $\lvert\eta\rvert$ <2.4	0.463	0.235	0.127	0.090
only 1 extra jet, $E_T^{raw} > 20$ GeV, $\lvert\eta\rvert$ <2.4	0.661	0.817	0.863	0.855
Factorised inside group 3: $M_{\tau\tau}$ reco and b tagging				
$E_{\tau 1,\tau 2} > 0$	0.921	0.898	0.882	0.834
$E_{\nu 1,\nu 2} > 0$	0.701	0.683	0.657	0.625
Total mass reconstruction	0.646	0.613	0.579	0.522
b tagging of the extra jet	0.098	0.050	0.033	0.016
$M_{\tau\tau}$ window: 150-300 GeV/c^2	0.142	0.295	0.433	0.430
$\varepsilon_{\text{Group3}}/\varepsilon_{\text{Group1}}$	2.77×10^{-3}	1.75×10^{-3}	9.15×10^{-4}	2.28×10^{-4}
$\varepsilon_{\text{Group1}} \times \varepsilon_{\text{Group2}} \times \varepsilon_{\text{Group3}}$	2.44×10^{-8}	6.07×10^{-8}	7.98×10^{-8}	2.84×10^{-8}
σ after selections (fb)	0.69	1.28	1.35	0.144
number of events for 60 fb^{-1}	41.4	76.7	81.2	8.7

Table 5.13: The number of expected events with 60 fb^{-1} and efficiencies of some of the selections for the irreducible backgrounds.

process	$N_{exp.}$ at 60fb^{-1}	$Q_{\tau 1} \times Q_{\tau 2}$ =-1	only one extra jet	b tag. jet	$M_{\tau\tau}$ window
$t\bar{t}$	0.64	0.96	0.36	0.42	0.11
W+j	0.33	0.81	0.15	0.06	0.12
Wt	0.26	0.96	0.49	0.44	0.23
$Z/\gamma^* \to \tau\tau$ in bins of generated $m_{\tau\tau}$					
130$< m_{\tau\tau} <$ 300 GeV/c^2	3.80	0.96	0.23	0.06	0.61
$m_{\tau\tau} >$300 GeV/c^2	0.18	0.95	0.27	0.05	0.04
$\tau\tau b\bar{b}$, $m_{\tau\tau} >$ 100 GeV/c^2	0.86	0.98	0.39	0.44	0.38

Tracker misalignment.

The effect of the tracker misalignment on the rate of fake τ-jets from the QCD multi-jet background was studied for the first data taking scenario (Scenario 1) and the long term data taking scenario (Scenario 2). The tracker isolation efficiency and the efficiency of the track counting in the signal cone (one or three tracks requirement) was compared with the performance of the perfect tracker alignment (Scenario 0).

It was found that in the Scenario 2 the QCD multi-jet background can be increased by $\simeq 11\%$ due to the change of the tracker isolation efficiency. The efficiency of the requirement to have one track in the signal cone is increased by $\simeq 10\%$ in the Scenario 2 relative to the perfect alignment.

The measurement of the QCD multi-jet background from the data.

Figure 5.3 (left plot) shows the expected $M_{\tau\tau}$ distribution for two signal samples and the background. The QCD multi-jet background is the biggest background in this analysis. The following way to evaluate this background from the data is proposed: A control sample must be used where all signal selections are applied except the mass window and the requirement to have an opposite charge of the two τ-jet candidates. It is proposed to select, instead, the sample with the same charge of the two τ-jet candidates (SS sample). The contamination of the signal events and irreducible background is negligible in the SS sample, thus giving the possibility to predict from the data the QCD multi-jet background in a given mass window from the number of event and the measured shape of the diτ-jet mass in SS sample. The expected number of QCD multi-jet SS events after all selections, but the mass window, used for the signal of M_A=200 GeV/c^2 is 380 with 60 fb^{-1}. Neglecting the uncertainty of the measured shape of the diτ-jet mass leads to 5% statistical uncertainty of the QCD multi-jet background estimates under the signal mass window. For the M_A=500 (800) GeV/c^2 selections about 80 (28) SS QCD multi-jet events are expected, thus giving $\simeq$ 10 (20) % statistical uncertainty.

5.2.6.5 Discovery reach in the $M_A - \tan\beta$ plane

Table 5.14 shows the lowest value of $\tan\beta$ for the three Higgs boson masses considered in the analysis, where the 5σ discovery is possible with 60 fb^{-1}. It is shown with and without QCD multi-jet background systematic uncertainty taken into account. The significance of the discovery is calculated with the S_{cP} method.

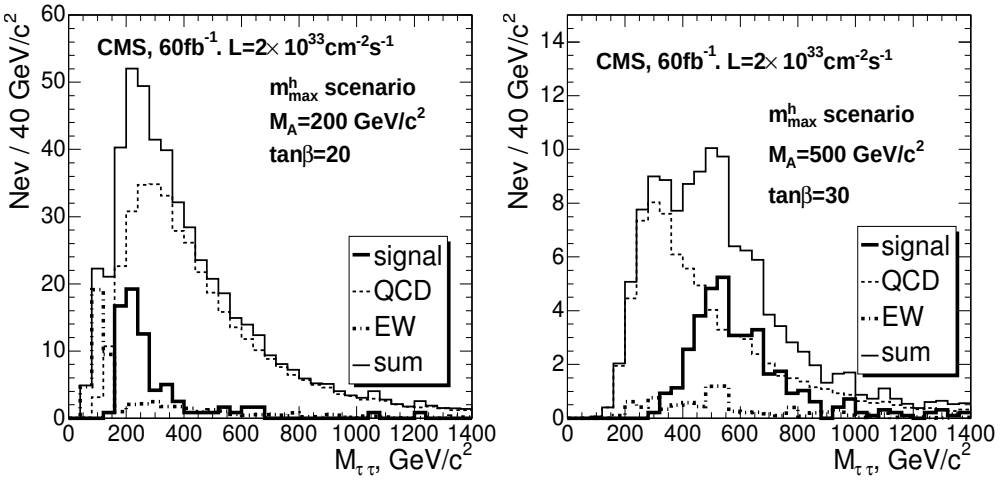

Figure 5.3: The expected $\mathrm{M}_{\tau\tau}$ distributions for the signal of $\mathrm{M_A}$=200 GeV/c^2, $\tan\beta$ =20 (left plot) and $\mathrm{M_A}$=500 GeV/c^2, $\tan\beta$ =30 (right plot) and the background with 60 fb^{-1}. Thick solid histogram - signal in the $\mathrm{m_h^{max}}$ scenario; dashed histogram - the QCD multi-jet background; thick dashed-dotted histogram - the irreducible background; normal solid histogram - signal plus background.

Table 5.14: The lower limit of $\tan\beta$ where a 5σ discovery is possible with 60 fb^{-1}.

low $\tan\beta$ limit	Higgs boson mass		
for 5σ discovery	$\mathrm{m_A}$ = 200 GeV/c^2	$\mathrm{m_A}$ = 500 GeV/c^2	$\mathrm{m_A}$ = 800 GeV/c^2
no systematics	20	32	46
with systematics	21	34	49

The extension of the discovery reach to lower values of $\tan\beta$ would be possible with a lower threshold on the energy of the additional jet in the event, provided that the fake jets will be then suppressed with the jet-tracks matching criteria. Another improvement is expected from the increase of the Higgs boson mass reconstruction efficiency using the improved missing $\mathrm{E_T}$ measurement from energy-flow like algorithms. Finally, improved b-jet tagging performance is expected to extend the discovery reach to lower values of $\tan\beta$.

5.2.7 $\mathrm{H} \to \tau\tau \to \mu + \mathrm{jet}$ analysis

A detailed description of the analysis can be found in [151].

5.2.7.1 Event generation and pre-selections

For the irreducible Drell Yan (DY) $\tau\tau$ background the $\tau_{1(2)} \to \mu\nu\nu$, $\tau_{2(1)} \to \mathrm{hadrons} + \nu$ decays were forced in PYTHIA. The events containing b quarks were rejected to avoid the double counting with the $\tau\tau\mathrm{b\bar{b}}$ background. For the other background processes, $\mathrm{t\bar{t}}$, Wt, W+jet and $\mathrm{b\bar{b}}$ no specific decay mode was forced.

The DY $\tau\tau$ background was produced in two ranges of the $\tau\tau$ invariant mass: $40 < \mathrm{m}_{\tau\tau} < 120\,\mathrm{GeV/c^2}$ and $\mathrm{m}_{\tau\tau} > 120\,\mathrm{GeV/c^2}$. For $\tau\tau\mathrm{b\bar{b}}$ the following mass bins were used: $60 < \mathrm{m}_{\tau\tau} < 100\,\mathrm{GeV/c^2}$ and $\mathrm{m}_{\tau\tau} > 100\,\mathrm{GeV/c^2}$. The W+jet background was generated with $\hat{p_\mathrm{T}} > 20\,\mathrm{GeV/c^2}$.

The SUSY background has been estimated using the events for the LM2 mSUGRA test point (see Section 13.3.2) with the total NLO SUSY cross section of 9.4 pb. For this point $\tan\beta = 35$, which makes the stau and tau production rate potentially dangerous. The number of events after all selection has been estimated to be less than one, therefore the SUSY background has been considered negligible, and was not studied in detail.

For the signal generation the Higgs boson was forced to decay into a τ pair. The τ leptons were decayed using TAUOLA and events with $\tau_{1(2)} \to \mu\nu\nu$, $\tau_{2(1)} \to$ hadrons $+ \nu$ decays were selected.

The pre-selections at generation level were chosen in a way that selected events are likely to pass the trigger selection. The requirements were: The isolation of the muon was defined as absence of charged particles with $\mathrm{p_T} > 1\,\mathrm{GeV/c}$ within a cone of radius 0.2 in the $\eta - \varphi$ space around the muon momentum direction. Isolation for the τ-like jet allowed for at most one charged particle with $\mathrm{p_T} > 1\,\mathrm{GeV/c}$ in the ring with an inner radius of 0.1 and an outer radius of 0.4 around the highest p_T charged particle in the jet. The leading track was required to have $p_\mathrm{T} > 3\,\mathrm{GeV/c}$. The $\tau\tau\mathrm{b\bar{b}}$ events were generated without the pre-selection requirements.

Details on $\mathrm{b\bar{b}}$ generation are explained in [152].

5.2.7.2 Event selection

The off-line τ-jet identification uses the parameters of the pixel HLT τ isolation, but with fully reconstructed tracks instead of pixel tracks. Additionally one or three tracks are required in the signal cone. For the τ-jet direction, the sum of the momenta of the signal tracks was used, improving the direction resolution. The leading τ-jet track is required to have $p_\mathrm{T} > 10\,\mathrm{GeV/c}$ in case of one track in the signal cone, and $p_\mathrm{T} > 20\,\mathrm{GeV/c}$ for three tracks, in order to suppress the $\mathrm{b\bar{b}}$ and DY $\tau\tau$ backgrounds.

To select events with associated $\mathrm{b\bar{b}H(A)}$ production, one b-tagged jet with calibrated $E_\mathrm{T} >$

20 GeV was required. For the b tagging, the track counting method was used [150]: the jet is b tagged if it has at least two tracks with a 2D transverse impact parameter significance greater than two. The b tagging efficiency, including the jet finding, for the signal is 17% for $M_A = 200\,GeV/c^2$ and 27% for $M_A = 500\,GeV/c^2$. For the backgrounds with a real b-jet it is 67% for $t\bar{t}$ and 46% for Wt processes. For the backgrounds without a real b-jet the mistagging efficiency is 1% for the W+jet and 3% for the DY $\tau\tau$ processes. The b tagging purity for the signal and the $t\bar{t}$ background is 95%; it is 90% for the Wb and the $\tau\tau b\bar{b}$ processes.

Events containing W bosons decaying into $\mu + \nu_\mu$ are suppressed using a cut on the transverse mass of the muon and the missing transverse energy: $m_T = \sqrt{2 \cdot p_T^\mu \cdot \not{E}_T (1 - \cos(\vec{p}_T^{\,\mu}, \vec{\not{E}}_T))}$, where $\not{E}_T$ is the missing transverse energy. The distribution of m_T has a Jacobian peak near the W mass. Rejecting events with $m_T > 60\,GeV$ largely reduces the $t\bar{t}$, Wt and W+jet backgrounds while retaining a good fraction of the signal events.

The additional selection against the $t\bar{t}$ background is the central jet veto. All events containing an additional jet (to the τ jet and the b-tagged jet) in the central region, $|\eta|$ <2.5, and with a calibrated $E_T > 20\,GeV$ were rejected.

The electrons from the W boson decays in the $t\bar{t}$ and Wt backgrounds can be misidentified as τ-jets. For the electron rejection a cut on the ratio of the τ-jet energy measured in the HCAL (E^{HCAL}) to the leading track momentum (p^{ltr}), f=E^{HCAL}/p^{ltr}, was used for the events with one track in the signal cone. The cut f> 0.2 retains 90% of the signal events, while it rejects 95% of the events with the real electrons. The cut on the upper value of the ratio is efficient against jets with a large fraction of neutral hadrons. The requirement f<1.1 rejects 50% of W+j and $b\bar{b}$ events and only 20% of signal events. Figure 5.4 shows the integrated distribution of the parameter f for the signal and the background events selected by the High Level trigger. The labels on the right part of the figure are ordered by decreasing selection efficiency in the acceptance region of 0.2<f< 1.1, marked by the arrows.

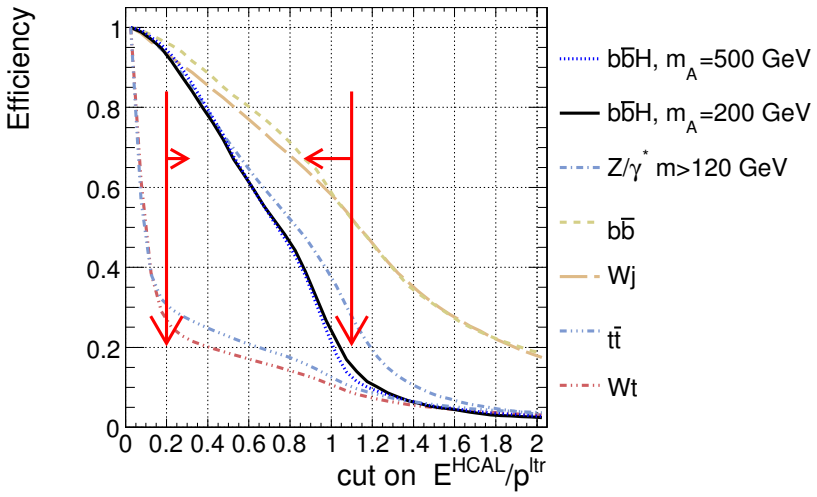

Figure 5.4: The integrated distribution of the parameter f=E^{HCAL}/p_T^{ltr}. The acceptance region of 0.2<f< 1.1 is marked by the arrows.

.

The Higgs boson mass reconstruction requires the rejection of events with a μ and a τ jet in a back-to-back topology, therefore the cut $\cos(\Delta\varphi(\vec{p}_T, \vec{E}_T^{\,jet})) > -0.9962$ was used. In ad-

dition, an upper cut on $\cos(\Delta\varphi(\vec{\mathrm{p}}_T, \vec{\mathrm{E}}_T^{jet})) < -0.5$ was used, retaining most of the signal events, while visibly reducing a fraction of the background events. Finally, the events with a negative reconstructed neutrino energy were rejected.

5.2.7.3 Expected number of selected events

Table 5.15 presents the production cross sections in fb and the individual selection efficiencies for signals of $\mathrm{M_A}$= 200 and 500 GeV/c^2. The signal cross sections and the branching ratios were obtained for the $\mathrm{m_h^{max}}$ scenario with μ=200 GeV (see Section 11.3.1). Tables 5.16-5.18 summarise the cross sections and the individual selection efficiencies for the background processes. The total efficiency of all selections and the cross sections after all selections are also presented at the end of the tables. The events were counted in the $\mathrm{M}_{\tau\tau}$ mass windows

Table 5.15: The production cross sections, in fb, and the individual selection efficiencies for the signal.

	$gg \to b\bar{b}(A+H), A, H \to \tau\tau$	
	$\mathrm{M_A}$=200 GeV/c^2 tan(β)=20	$\mathrm{M_A}$=500 GeV/c^2 tan(β)=30
$\sigma\times$ BR [fb]	$9.12 \cdot 10^3$	$4.51 \cdot 10^2$
kine pre-selection	$9.47 \cdot 10^{-2}$	$1.65 \cdot 10^{-1}$
Level-1 trigger	$8.99 \cdot 10^{-1}$	$9.09 \cdot 10^{-1}$
HLT	$4.17 \cdot 10^{-1}$	$4.99 \cdot 10^{-1}$
offline τ-jet isolation	$9.54 \cdot 10^{-1}$	$9.60 \cdot 10^{-1}$
1 or 3 tk. in τ-jet signal cone	$9.12 \cdot 10^{-1}$	$9.19 \cdot 10^{-1}$
$\mathrm{p_T^{ltr}}$ >10 GeV/c	$9.05 \cdot 10^{-1}$	$9.55 \cdot 10^{-1}$
$Q_\mu \cdot Q_{jet} = -1$	$9.61 \cdot 10^{-1}$	$9.60 \cdot 10^{-1}$
single b tagging	$1.73 \cdot 10^{-1}$	$2.56 \cdot 10^{-1}$
no jet with $E_T > 20$, $\lvert\eta\rvert < 2.5$	$8.53 \cdot 10^{-1}$	$7.72 \cdot 10^{-1}$
$m_T(l, MET) < 60\ GeV$	$8.33 \cdot 10^{-1}$	$7.01 \cdot 10^{-1}$
$-0.996 < cos(\Delta\varphi) < -0.5$	$8.05 \cdot 10^{-1}$	$7.51 \cdot 10^{-1}$
electron veto: $0.2 < f < 1.1$	$8.22 \cdot 10^{-1}$	$8.54 \cdot 10^{-1}$
$E_{\nu 1} > 0, E_{\nu 2} > 0$	$6.84 \cdot 10^{-1}$	$7.68 \cdot 10^{-1}$
total efficiency:	$1.66 \cdot 10^{-3}$	$4.53 \cdot 10^{-3}$
σ after selections [fb]:	$1.52 \cdot 10^1$	2.05

with the width taken to be $\pm\sigma$, where σ is given by the standard deviation of a Gaussian fit of the signal $\mathrm{M}_{\tau\tau}$ distributions. The value of σ is 41 GeV/c^2 for $\mathrm{M_A} = 200$ GeV/c^2 , whereas it is 83 GeV/c^2 for $\mathrm{m_A} = 500$ GeV/c^2. With an integrated luminosity of 20 fb^{-1} the expected number of signal (background) events is 146 (127) for $\mathrm{m_A} = 200$ GeV/c^2, $\tan\beta = 20$, and 21 (61) for $\mathrm{m_A} = 500$ GeV/c^2, $\tan\beta = 30$. Figure 5.5 shows the expected $\tau\tau$ mass distribution for the total background and for the signal plus background for $\mathrm{M_A} = 200$ GeV/c^2, $\tan\beta = 20$ and $\mathrm{M_A} = 500$ GeV/c^2, $\tan\beta = 30$.

5.2.7.4 Background estimates and uncertainty

After all off-line selections the main background is represented by the $\tau\tau\mathrm{b\bar{b}}$, DY $\tau\tau$ and the $\mathrm{t\bar{t}}$ production processes. The contribution of the non Z/γ^* background, mainly the $\mathrm{t\bar{t}}$ events, can be estimated applying the inversion of the electron veto: f<0.1 instead of 0.2<f<1.1. All

Table 5.16: The production cross sections, in fb, and the individual selection efficiencies for the reducible background processes.

	$t\bar{t}$	$W + jet$	Wt	$b\bar{b}$
σ [fb]	$8.40 \cdot 10^{5}$	$4.15 \cdot 10^{7}$	$6.20 \cdot 10^{4}$	$2.29 \cdot 10^{10}$
kine preselection	$9.01 \cdot 10^{-2}$	$1.44 \cdot 10^{-2}$	$6.58 \cdot 10^{-2}$	$7.56 \cdot 10^{-4}$
Level-1 trigger	$9.06 \cdot 10^{-1}$	$8.40 \cdot 10^{-1}$	$8.91 \cdot 10^{-1}$	$2.26 \cdot 10^{-2}$
HLT	$9.61 \cdot 10^{-2}$	$4.16 \cdot 10^{-2}$	$1.05 \cdot 10^{-1}$	$2.36 \cdot 10^{-4}$
offline τ-jet isolation	$8.51 \cdot 10^{-1}$	$6.70 \cdot 10^{-1}$	$8.79 \cdot 10^{-1}$	$8.69 \cdot 10^{-1}$
1 or 3 tk. in τ-jet signal cone	$8.92 \cdot 10^{-1}$	$6.30 \cdot 10^{-1}$	$9.07 \cdot 10^{-1}$	$7.19 \cdot 10^{-1}$
$\mathrm{p_T^{ltr}}$ >10 GeV/c	$9.42 \cdot 10^{-1}$	$8.58 \cdot 10^{-1}$	$9.37 \cdot 10^{-1}$	$7.17 \cdot 10^{-1}$
$Q_\mu \cdot Q_{jet} = -1$	$9.18 \cdot 10^{-1}$	$7.31 \cdot 10^{-1}$	$9.52 \cdot 10^{-1}$	$5.45 \cdot 10^{-1}$
single b tagging	$6.73 \cdot 10^{-1}$	$1.09 \cdot 10^{-2}$	$4.56 \cdot 10^{-1}$	$9.42 \cdot 10^{-2}$
no jet with $E_T > 20$, $\lvert\eta\rvert < 2.5$	$3.43 \cdot 10^{-1}$	$8.17 \cdot 10^{-1}$	$8.60 \cdot 10^{-1}$	$4.30 \cdot 10^{-1}$
$m_T(l, MET) < 60$ GeV/c^2	$3.53 \cdot 10^{-1}$	$3.76 \cdot 10^{-1}$	$3.62 \cdot 10^{-1}$	1.00
$-0.996 < cos(\Delta\varphi) < -0.5$	$4.95 \cdot 10^{-1}$	$6.56 \cdot 10^{-1}$	$4.51 \cdot 10^{-1}$	$4.16 \cdot 10^{-1}$
electron veto: $< 0.2 < f < 1.1$	$1.65 \cdot 10^{-1}$	$4.76 \cdot 10^{-1}$	$1.27 \cdot 10^{-1}$	$2.98 \cdot 10^{-1}$
$E_{\nu 1} > 0, E_{\nu 2} > 0$	$4.08 \cdot 10^{-1}$	$2.00 \cdot 10^{-1}$	$4.15 \cdot 10^{-1}$	$3.60 \cdot 10^{-1}$
total efficiency:	$1.54 \cdot 10^{-5}$	$3.31 \cdot 10^{-8}$	$1.66 \cdot 10^{-5}$	$7.86 \cdot 10^{-11}$
σ after selections [fb]:	$1.30 \cdot 10^{1}$	1.37	1.03	1.80

Table 5.17: The production cross sections, in fb, and the individual selection efficiencies for the irreducible background processes.

	$Z/\gamma^* \to \tau\tau \to \mu + \mathrm{jet}$	
	$40 < m_{\tau\tau} < 120$ GeV/c^2	$m_{\tau\tau} > 120$ GeV/c^2
$\sigma\times$ BR [fb]	$4.63 \cdot 10^{5}$	$4.88 \cdot 10^{3}$
kine preselection	$6.56 \cdot 10^{-2}$	$2.14 \cdot 10^{-1}$
Level-1 trigger	$8.00 \cdot 10^{-1}$	$8.28 \cdot 10^{-1}$
HLT	$1.03 \cdot 10^{-1}$	$2.77 \cdot 10^{-1}$
offline τ-jet isolation	$9.12 \cdot 10^{-1}$	$9.40 \cdot 10^{-1}$
1 or 3 tk. in τ-jet signal cone	$9.03 \cdot 10^{-1}$	$8.93 \cdot 10^{-1}$
$\mathrm{p_T^{ltr}}$ >10 GeV/c	$8.12 \cdot 10^{-1}$	$9.00 \cdot 10^{-1}$
$Q_\mu \cdot Q_{jet} = -1$	$9.47 \cdot 10^{-1}$	$9.33 \cdot 10^{-1}$
single b tagging	$2.68 \cdot 10^{-2}$	$2.51 \cdot 10^{-2}$
no jet with $E_T > 20$, $\lvert\eta\rvert < 2.5$	$7.77 \cdot 10^{-1}$	$6.98 \cdot 10^{-1}$
$m_T(l, MET) < 60$ GeV/c^2	$9.41 \cdot 10^{-1}$	$7.74 \cdot 10^{-1}$
$-0.996 < cos(\Delta\varphi) < -0.5$	$3.75 \cdot 10^{-1}$	$6.57 \cdot 10^{-1}$
electron veto: $0.2 < f < 1.1$	$6.46 \cdot 10^{-1}$	$7.29 \cdot 10^{-1}$
$E_{\nu 1} > 0, E_{\nu 2} > 0$	$6.45 \cdot 10^{-1}$	$6.46 \cdot 10^{-1}$
total efficiency:	$1.31 \cdot 10^{-5}$	$1.75 \cdot 10^{-4}$
σ after selections [fb]:	6.08	$8.53 \cdot 10^{-1}$

other cuts must be the same, including the $\mathrm{M}_{\tau\tau}$ mass window. A relatively pure sample of $\mathrm{t\bar{t}}$ can be selected, since the requirement f<0.1 rejects more than 95% of all processes except the

Table 5.18: The production cross sections, in fb, and the individual selection efficiencies for the irreducible background processes.

	$bb(Z \to \tau\tau)$	
	$60 < m_{\tau\tau} < 100\,\text{GeV/c}^2$	$m_{\tau\tau} > 100\,\text{GeV/c}^2$
$\sigma\times$ BR [fb]	$2.61 \cdot 10^4$	$1.05 \cdot 10^3$
kine preselection	1.00	1.00
Level-1 trigger	$1.41 \cdot 10^{-1}$	$1.64 \cdot 10^{-1}$
HLT	$4.10 \cdot 10^{-3}$	$1.21 \cdot 10^{-2}$
offline τ-jet isolation	$9.05 \cdot 10^{-1}$	$9.34 \cdot 10^{-1}$
1 or 3 tk. in τ-jet signal cone	$9.12 \cdot 10^{-1}$	$9.17 \cdot 10^{-1}$
p_T^{ltr} >10 GeV/c	$8.60 \cdot 10^{-1}$	$8.98 \cdot 10^{-1}$
$Q_\mu \cdot Q_{jet} = -1$	$9.41 \cdot 10^{-1}$	$9.48 \cdot 10^{-1}$
single b tagging	$2.73 \cdot 10^{-1}$	$2.75 \cdot 10^{-1}$
no jet with $E_T > 20$, $\lvert\eta\rvert < 2.5$	$7.20 \cdot 10^{-1}$	$7.72 \cdot 10^{-1}$
$m_T(l, MET) < 60\,\text{GeV}$	$9.68 \cdot 10^{-1}$	$8.80 \cdot 10^{-1}$
$-0.996 < cos(\Delta\varphi) < -0.5$	$4.23 \cdot 10^{-1}$	$5.84 \cdot 10^{-1}$
electron veto: $0.2 < f < 1.1$	$6.98 \cdot 10^{-1}$	$5.11 \cdot 10^{-1}$
$E_{\nu 1} > 0, E_{\nu 2} > 0$	$4.32 \cdot 10^{-1}$	$5.62 \cdot 10^{-1}$
total efficiency:	$6.64 \cdot 10^{-5}$	$2.76 \cdot 10^{-4}$
σ after selections [fb]:	1.74	$2.89 \cdot 10^{-1}$

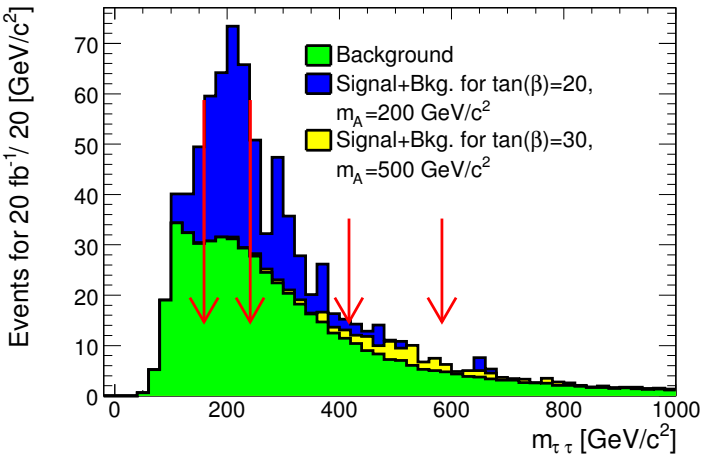

Figure 5.5: The reconstructed $\tau\tau$ mass distribution. The signal and the background contributions are shown with 20 fb^{-1}. The mass windows in which the events are counted for the significance calculations are shown.

$t\bar{t}$ and Wt as shown in Fig. 5.4. The number of the non Z/γ^* background events in the signal region can be then predicted using the ratio of the $t\bar{t}$ events in the signal region of 0.2<f<1.1 and in the region of f<0.1. This ratio can be obtained from Monte-Carlo simulation or from real $t\bar{t}$ data. The systematic uncertainty on the number of the non Z/γ^* background events predicted using this method has two contributions:

- The uncertainty of the HCAL energy scale, since the variable $f=E^{HCAL}/p^{ltr}$ includes the HCAL part of the τ-jet candidate energy measured by the calorimeter.

It is taken as 3%.

- The uncertainty of the shape of the distribution of f. The shape is obtained from $\mathrm{t\bar{t}}$ events only, however a small fraction of events from the other processes is present in the "normalisation" region of f<0.1. It leads to an uncertainty of $\simeq$ 12 %.

The contribution from the other systematic uncertainties, e.g. b tagging is expected to be small, due to the cancellation in the efficiency ratio. The total uncertainty on the number of the non Z/γ^* background events is thus 12.4 %.

The Z/γ^* background consists of two parts: the $\tau\tau\mathrm{b\bar{b}}$ process and the DY $\tau\tau$ process without genuine b quarks in the event. The DY $\tau\tau$ background can be predicted using the DY $\ell\ell$ (ℓ = e, μ) cross section, to be measured with high precision at LHC, and the selection efficiency obtained from the Monte-Carlo. The systematic uncertainty on the number of DY $\tau\tau$ events has two main contributions due to:

- The jet scale uncertainty. The number of the events in the $\mathrm{M}_{\tau\tau}$ signal window varies by $\pm$6% for jet scale variations of $\pm 3\%$ and missing transverse energy scale variations of $\pm$ 5%.
- The b-mistagging uncertainty. A conservative estimate of 5% is taken.

The total uncertainty on the number of the DY $\tau\tau$ events with the jet mistagged as a b-jet is therefore 8%.

For the $\tau\tau\mathrm{b\bar{b}}$ background estimates the systematic uncertainty has the following main contributions:

- The uncertainty of the $\mu\mu\mathrm{b\bar{b}}$ cross section measurement (without the luminosity uncertainty) is 14% [144].
- The jet scale uncertainty. It is assumed to be the same as for the DY $\tau\tau$ events.

The total uncertainty on the number of the $\tau\tau\mathrm{b\bar{b}}$ events is 15%.

5.2.7.5 Discovery reach in the $\mathrm{M_A} - \tan\beta$ plane

The CMS discovery reach in the $\mathrm{M_A} - \tan\beta$ plane with 30 fb^{-1} in the $\mathrm{m_h^{max}}$ scenario is shown in the Fig. 5.6. The 5 σ discovery curves are shown without (lower curve) and with (upper curve) the uncertainty on the background taken into account.

5.2.8 $\mathrm{H} \to \tau\tau \to e + \mathrm{jet}$ analysis

A detailed description of the analysis can be found in [153].

5.2.8.1 Event generation

The signal process $\mathrm{gg} \to \mathrm{bbH/A}$, $\mathrm{H/A} \to \tau\tau$, $\tau_1 \to \mathrm{e}\nu_\mathrm{e}\nu_\tau$, $\tau_2 \to \tau\ \mathrm{jet} + \nu_\tau$ leads to a final state of one isolated electron, an isolated τ jet and one or two detectable b jets. The background with genuine τ's is due to two types of events, Z/γ^* events decaying into $\tau\tau$, and the $\mathrm{t\bar{t}}$ events, where the $\mathrm{e} + \tau\ \mathrm{jet}$ final state can come from direct W decays to an electron and a τ or through $\mathrm{W} \to \tau\nu_\tau \to \mathrm{e}\nu_\mathrm{e}\nu_\tau\nu_\tau$ decays:

- $\mathrm{Z}/\gamma^* \to \tau\tau \to \mathrm{e} + \tau\ \mathrm{jet} + \mathrm{X}$
- $\mathrm{b\bar{b}Z}/\gamma^*, \mathrm{Z}/\gamma^* \to \tau\tau \to \mathrm{e} + \tau\ \mathrm{jet} + \mathrm{X}$
- $\mathrm{t\bar{t}}$ with $\mathrm{W}_1 \to \tau\nu_\tau$ ($\tau \to$ jet), $\mathrm{W}_2 \to \mathrm{e}\nu_\mathrm{e}$ or $\mathrm{W}_2 \to \tau\nu_\tau \to \mathrm{e}\nu_\mathrm{e}\nu_\tau\nu_\tau$.

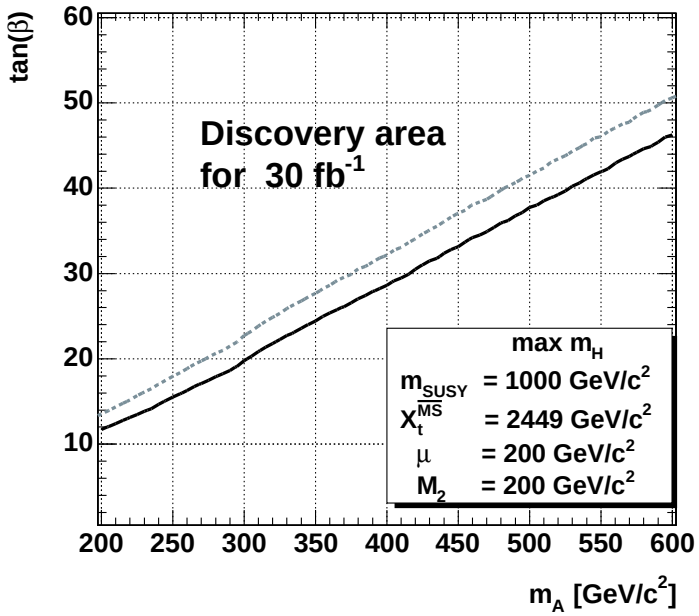

Figure 5.6: The 5 σ discovery region in the $\mathrm{M_A} - \tan\beta$ plane with 30 fb^{-1} of the integrated luminosity for the $\mathrm{m_h^{max}}$ MSSM scenario. The regions are shown without (lower curve) and with (upper curve) the uncertainty on the background taken into account.

- Wt, with $\mathrm{W_1} \to \tau\nu_\tau$ ($\tau \to$ jet), $\mathrm{W_2} \to \mathrm{e}\nu_\mathrm{e}$ or $\mathrm{W_2} \to \tau\nu_\tau \to \mathrm{e}\nu_\mathrm{e}\nu_\tau\nu_\tau$.

Background can arise also from the processes where a hadronic jet or an electron leads to a fake τ:

- W+jet, with $\mathrm{W} \to \mathrm{e}\nu_\mathrm{e}$
- $\mathrm{Z}/\gamma^* \to \mathrm{e^+e^-}$
- $\mathrm{b\bar{b}Z}/\gamma^*, \mathrm{Z}/\gamma^* \to \mathrm{e^+e^-}$
- $\mathrm{t\bar{t}}$ with $\mathrm{W} \to$ jj or $\mathrm{W} \to \mathrm{e}\nu_\mathrm{e}$.

The QCD multi-jet production is a large potential background through hadronic jets faking both the electron and the τ jet.

For the inclusive Z/γ^* production the events containing b quarks in the final state were removed to avoid double counting with the $\tau\tau\mathrm{b\bar{b}}$ background. The single top (Wt) events were generated with TOPREX [44]. The τ decays in the signal were performed with the TAUOLA package [154].

5.2.8.2 Event selection

In the offline reconstruction an isolated electron from the decay of one of the τ's was first searched for. On the average ~ 1.3 reconstructed electron candidates were found in the signal events. The reconstructed electrons were first required to be isolated in the tracker demanding that no track with $\mathrm{p_T} > 1\,\mathrm{GeV/c}$ was found in a cone of $\Delta\mathrm{R} = 0.4$ around the electron candidate direction. The further electron identification was performed following the algo-

rithm of Ref. [155]. The largest contribution to the identification efficiency and purity was obtained from the ratio of hadronic cluster energy to the electromagnetic energy of the cluster ($E^{hadronic}/E^{elm} < 0.2$) and from the ratio of the supercluster energy to the track momentum ($E^{super\ cluster}/p^{track} > 0.8$). The identification efficiency, including the tracker isolation, was found to be 64.2%. A good purity of 97.5% was obtained for the selected electrons.

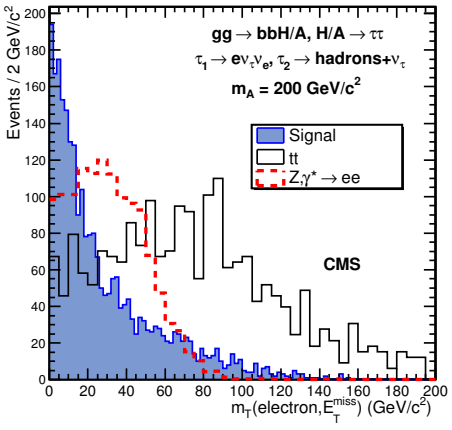

Figure 5.7: Distribution of transverse mass reconstructed from the electron and the missing transverse energy for the signal of M_A = 200 GeV/c^2 and $\tan\beta$ = 20 (filled histogram), for the $t\bar{t}$ (solid line) and for the $Z/\gamma^* \to e^+e^-$ (dashed line) background. Histogram normalisation is arbitrary.

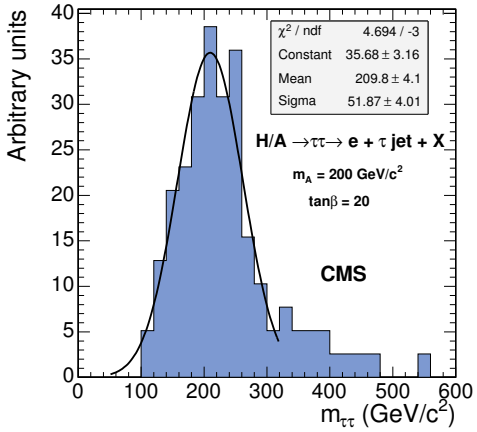

Figure 5.8: Reconstructed Higgs boson mass for M_A = 200 GeV/c^2 and $\tan\beta$ = 20.

The off-line τ-jet identification was applied to the jets with $E_T^{jet} > 40$ GeV reconstructed in the calorimeter with the cone of 0.4. The leading track with $p_T^{ltr} > 10$ GeV/c was searched for in a cone of R_m=0.1 around the τ-jet direction. For an efficient isolation against the hadronic jets in the W+jet and QCD multi-jet backgrounds, a small signal cone, R_S=0.04, around the leading track was used. About 83% of the $\tau^\pm \to \text{hadron}^\pm + n\pi^0 + \nu_\tau$ decays were found to be reconstructed as one prong τ's. Due to the small signal cone selected, 50% of the $\tau^\pm \to 3\ \text{hadrons}^\pm + n\pi^0 + \nu_\tau$ decays were reconstructed as one or two prong τ-jets. The cut $p_T^{ltr} > 20$ GeV/c was found to be optimal for the suppression of the hadronic jets, in the presence of the QCD multi-jet background. The isolation was performed counting tracks with $p_T^i > 1$ GeV/c in the area between the signal cone and the isolation cone, which was taken to be then same as the jet reconstruction cone, R_i = 0.4. Following the method described in [145], at least eight hits were required in the full silicon tracker and an upper bound of 0.3 mm on the transverse impact parameter was set on the leading track in order to suppress the background from the fake tracks.

The $Z/\gamma^* \to e^+e^-$ and $b\bar{b}Z/\gamma^*, Z/\gamma^* \to e^+e^-$ backgrounds contain an isolated genuine electron to pass the electron cuts and are not significantly suppressed with the τ-selection cuts. These electronic τ candidates were suppressed requiring a large energy deposition in the hadron calorimeter. A cut in the E_T of the most energetic HCAL cell in the τ jet, $E_T(\text{max HCAL cell}) > 2$ GeV, was found to suppress the electrons with a factor of ~ 7. A further reduction was obtained comparing the HCAL energy and the leading track momentum of the τ jet. The cut $E^{HCAL}/p^{ltr} > 0.35$, applied on the one-prong τ candidates only,

was found to suppress further the electronic τ candidates by a factor of ~ 1.8. The W+jet events show a tail at large values of $\mathrm{E^{HCAL}/p^{ltr}}$ due to the neutral hadron component of the hadronic jets and were suppressed with the cut $\mathrm{E^{HCAL}/p^{ltr}} < 1.5$.

Efficiencies of the τ-jet selections are shown in Tables 5.19, 5.20 and 5.21. The purity of $\sim 97\%$ is obtained for the signal events. A rejection factor of ~ 400 was obtained for the QCD multi-jet events generated with $50 < \hat{\mathrm{p}}_{\mathrm{T}} < 80$ GeV/c when the τ-jet selections described above were applied.

Finally, the charges of the electron and τ jet were required to be opposite. The charge of the τ jet was calculated as the sum of charges of the tracks in the signal cone.

The missing transverse energy measurement can be exploited to suppress the $\mathrm{t\bar{t}}$ background with an upper bound on the transverse mass $\mathrm{m_T(e, E_T^{miss})}$ reconstructed from the electron and the missing transverse energy. Figure 5.7 shows the $\mathrm{m_T(e, E_T^{miss})}$ distribution for the signal events with $\mathrm{M_A}$ = 200 GeV/c^2 and for the $\mathrm{t\bar{t}}$ and $\mathrm{Z/\gamma^* \rightarrow e^+e^-}$ backgrounds with the electron and τ-jet selections. The selected upper bound $\mathrm{m_T(e, E_T^{miss})} < 40$ GeV/c^2 reduces the $\mathrm{t\bar{t}}$ background with a factor of ~ 4.

The events were further selected when at least one jet (in addition to the τ jet) with calibrated $\mathrm{E_T^{jet}} > 20$ GeV and $|\eta| < 2.5$ was found and tagged as the b jet. A probabilistic secondary vertex algorithm with a discriminator cut from Ref. [156] was used for b tagging. The cut in the discriminator was set to 0.8, which suppresses efficiently the $\mathrm{Z/\gamma^*}$, W+jet and the potential multi-jet background. The efficiency to tag at least one jet, including the jet finding efficiency, was found to be between 13 and 19% for the signal, below 1% for the $\mathrm{Z/\gamma^*}$ backgrounds and 1.3% for the W+jet background. For the signal events the purity of the b-tagged jets is very high (99%).

The $\mathrm{t\bar{t}}$ background, with a genuine electron, τ and b jets, can not be significantly suppressed with the cuts described above. This background, however, was suppressed applying the jet veto: the event must contain only the b-tagged jet with calibrated $\mathrm{E_T^{jet}} > 20$ GeV and $|\eta^{\mathrm{jet}}| < 2.5$. The fake jets, which generally do not contain tracks from the signal vertex, were suppressed with a cut in the fraction of the track $\mathrm{p_T}$ sum to the jet $\mathrm{E_T}$, $\alpha = \Sigma \mathrm{p_T^{track}/E_T^{jet}}$. The cut $\alpha > 0.1$ was found to improve the veto efficiency for the signal by about 10%. The jet veto efficiency is around 60% for the signal and $\sim 5\%$ for the $\mathrm{t\bar{t}}$ background.

For the reconstruction of the $\tau\tau$ mass the events with back-to-back configurations between the electron and the τ jet were removed with an upper bound on the angle between the τ jet and the electron in the transverse plane ($\Delta\varphi(\mathrm{e}, \tau\ \mathrm{jet})$). The reconstructed neutrino energies were required to be positive ($\mathrm{E}_{\nu_1} > 0$ and $\mathrm{E}_{\nu_2} > 0$), which leads to a reduction of $\simeq 40\%$ of the signal events, but rejects $\simeq 60\%$ of the $\mathrm{t\bar{t}}$, tW and W+jet backgrounds. Figure 5.8 shows the reconstructed Higgs boson mass for the signal events with $\mathrm{M_A}$ = 200 GeV/c^2. The Gaussian fit yields a mass resolution of 25%.

Table 5.19 shows the numbers of signal events with $\mathrm{M_A}$ = 130-500 GeV/c^2 and $\tan\beta$ = 20 for 30 fb^{-1} and the efficiency for all the event selection cuts described above. For $\mathrm{M_A} = 130$ and 140 GeV/c^2, the mass of the lighter scalar Higgs boson h is only 4.4 and 11.2 GeV/c^2 smaller than $\mathrm{M_A}$. With the mass resolution, which can be reached in the $\mathrm{H} \rightarrow \tau\tau$ decay channels, the lighter scalar contributes to the signal and is added in the cross sections for $\mathrm{M_A} = 130$ and 140 GeV/c^2. The contribution is 31 and 11% of the total production rate, respectively. Table 5.20 shows the number of events and efficiencies for the backgrounds

originating from $Z/\gamma^* \to \tau\tau$ and $Z/\gamma^* \to e^+e^-$ decays in the inclusive and in the associated $b\bar{b}Z/\gamma^*$ production. The efficiency of removing the $b\bar{b}Z/\gamma^*$ component from the inclusive Z/γ^* samples is also shown. Table 5.21 shows the same for the backgrounds involving W's from $t\bar{t}$, Wt and W+jet events. The cross section times branching fraction, trigger efficiency and the efficiency of the primary vertex reconstruction are also shown in the tables. The QCD multi-jet background after all selections was estimated to be 8.4 events for 30 fb^{-1} in the mass window around M_A = 200 GeV/c^2, which is $\simeq$ 10% of all other backgrounds.

Figures 5.9 to 5.10 show the reconstructed Higgs boson mass distributions of the $H/A \to \tau^+\tau^- \to$ electron + jet + X signal and the total background for 30 fb^{-1} for M_A = 200 GeV/c^2, $\tan\beta$ = 20 and for M_A = 300 GeV/c^2, $\tan\beta$ = 25. The sum of the $Z/\gamma^* \to e^+e^-$ and $b\bar{b}Z/\gamma^* \to e^+e^-$ backgrounds is shown separately in the figures.

5.2.8.3 Systematic uncertainties for the background determination

The background uncertainty was evaluated using the cross-section uncertainties (measured or predicted from the theory) and the experimental uncertainties for the event selections.

The uncertainty of the event selection efficiency is related to the uncertainty of the electron and τ identification, the absolute calorimeter scale and the b-tagging efficiency. The systematic uncertainty due to the energy scale was estimated varying the jet energy and the E_T^{miss} values with the expected energy scale uncertainties yielding an average 5.1% uncertainty on the number of Z/γ^* events, 3.8% uncertainty on the number of $b\bar{b}Z/\gamma^*$ events, 7.3% uncertainty on the number of $t\bar{t}$ events, 11.3% uncertainty on the number of tW events and 11.8% uncertainty on the number of W+jet events passing the event selection cuts. A 5% uncertainty on the b tagging and mistagging efficiencies and a 2% uncertainty on the electron reconstruction and identification were used.

The uncertainty of the Z/γ^* cross section at the LHC is of the order of 1% [157]. For the $t\bar{t}$ background the theoretical NLO cross section uncertainty derives from the scale uncertainty, taken to be 5% according to Ref. [158], and the PDF uncertainty, about 2.5 %, yielding 5.6

Table 5.19: Production cross sections times branching fraction, efficiencies (%) for the selection cuts and numbers of events for 30 fb^{-1} for the signal with $\tan\beta$ = 20 and for M_A = 130, 200, 300 and 500 GeV/c^2.

M_A (GeV/c^2)	130	200	300	500
$\sigma \times$ BR (pb)	18.2	4.15	0.85	0.071
Level-1 and HLT	1.53 (8.4)	0.64 (15.4)	0.18 (21.6)	2.0×10^{-2} (28.7)
primary vertex	1.44 (94.1)	0.60 (94.2)	0.18 (97.2)	1.9×10^{-2} (93.6)
electron identification	1.11 (77.8)	0.48 (80.8)	0.14 (73.7)	1.4×10^{-2} (73.8)
one identified τ jet	0.127 (11.4)	0.11 (23.4)	4.5×10^{-2} (32.9)	5.9×10^{-3} (41.7)
$Q^{\tau\ jet} \times Q^e$ = -1	0.127 (100.0)	0.11 (99.1)	4.5×10^{-2} (99.3)	5.8×10^{-3} (99.0)
$m_T < 40$ GeV/c^2	9.9×10^{-2} (77.6)	3.8×10^{-2} (73.7)	3.1×10^{-2} (69.3)	3.9×10^{-3} (66.7)
$\geq$1 jet, $E_T > 20$ GeV	4.5×10^{-2} (45.9)	3.8×10^{-2} (46.6)	1.5×10^{-2} (48.6)	2.1×10^{-3} (53.5)
b tagging	1.3×10^{-2} (29.7)	1.2×10^{-2} (32.2)	5.0×10^{-3} (32.9)	7.6×10^{-4} (36.5)
jet veto	8.1×10^{-3} (60.2)	7.2×10^{-2} (62.5)	3.1×10^{-3} (63.2)	4.6×10^{-4} (61.0)
$\Delta\varphi(\tau_1,\tau_2) < 175^o$	7.6×10^{-3} (94.8)	6.8×10^{-3} (93.9)	2.7×10^{-3} (85.7)	3.4×10^{-4} (74.5)
$E_{\nu_1,\nu_2} > 0$	4.1×10^{-3} (54.1)	4.2×10^{-3} (61.7)	1.7×10^{-3} (64.3)	2.4×10^{-4} (70.6)
N_{ev} at 30 fb^{-1}	123.9	126.0	51.9	7.3

Table 5.20: Background production cross sections times branching fraction, cross sections and efficiencies (%) for the selection cuts and number of events for 30 fb^{-1}.

	$Z/\gamma^* \to \tau\tau$	$b\bar{b}Z/\gamma^* \to \tau\tau$	$Z/\gamma^* \to e^+e^-$	$b\bar{b}Z/\gamma^* e^+e^-$
$\sigma \times$ BR (pb)	331.8	27.0	1890	26.3
pre-selection	173.5 (41.4)		811.2 (42.9)	
Level-1 and HLT	17.3 (10.0)	0.818 (3.1)	617.4 (76.1)	18.2 (67.2)
primary vertex	16.5 (95.4)	0.796 (97.3)	591.9 (95.9)	17.7 (97.3)
no b's in DY Z/γ^*	15.6 (94.6)		561.8 (94.9)	
electron identification	11.6 (74.4)	0.585 (80.2)	278.1 (50.1)	9.31 (52.6)
one identified τ jet	0.13 (1.2)	1.0×10^{-2} (1.8)	3.40 (1.2)	9.0×10^{-2} (1.0)
$Q^{\tau\ \mathrm{jet}} \times Q^e$ = -1	0.13 (96.3)	1.0×10^{-2} (100)	3.31 (97.4)	8.8×10^{-2} (97.8)
m_T <40 GeV/c^2	9.8×10^{-2} (76.3)	8.0×10^{-3} (80.0)	2.26 (68.3)	5.5×10^{-2} (62.5)
$\geq$1 jet, $E_T > 20$ GeV	4.0×10^{-2} (40.6)	5.6×10^{-3} (70.0)	0.85 (37.6)	3.0×10^{-2} (54.2)
b tagging	8.0×10^{-4} (2.0)	2.6×10^{-3} (46.4)	1.5×10^{-2} (1.8)	9.6×10^{-3} (32.2)
jet veto	5.2×10^{-4} (65.0)	1.5×10^{-3} (57.7)	6.0×10^{-3} (41.4	5.9×10^{-3} (67.4)
$\Delta\varphi(\tau_1,\tau_2) < 175^o$	4.9 $\times10^{-4}$ (94.2)	1.4×10^{-3} (90.7)	4.8×10^{-3} (80.0)	5.1×10^{-3} (85.7)
$E_{\nu_1,\nu_2} > 0$	2.0 $\times10^{-4}$ (40.2)	7.6×10^{-4} (55.9)	1.7×10^{-3} (35.4)	1.9×10^{-3} (50.0)
N_{ev} at 30 fb^{-1}	5.9	22.8	51.3	57.9

Table 5.21: Background production cross sections times branching fraction (pb), cross sections and efficiencies (%) for the selection cuts and number of events for 30 fb^{-1}.

	$t\bar{t}$	Wt	W+jet
$\sigma \times$ BR (pb)	840	6.16	673.2
pre-selection			315.0 (46.8)
Level-1 and HLT	94.4 (11.3)	2.00 (32.5)	145.6 (46.2)
primary vertex	93.9 (99.5)	1.97 (98.5)	143.9 (98.8)
electron identification	66.7 (71.0)	1.43 (72.6)	114.2 (79.4)
one id. τ jet	0.66 (0.95)	4.10×10^{-2} (2.87)	0.57 (0.5)
$Q^{\tau\ \mathrm{jet}} \times Q^e$ = -1	0.57 (89.8)	4.00×10^{-2} (97.6)	0.47 (82.7)
$m_T(e, E_T^{miss})$ <40 GeV/c^2	0.14 (24.3)	8.0×10^{-3} (20.0)	0.12 (25.2)
$\geq$1 jet, $E_T > 20$ GeV	0.14 (98.6)	6.9×10^{-3} (86.3)	5.5×10^{-2} (46.2)
b tagging	9.4×10^{-2}(68.6)	4.1×10^{-3} (59.4)	1.6×10^{-3} (2.9)
jet veto	5.1×10^{-3} (5.4)	2.38×10^{-3} (58.1)	6.6×10^{-4} (41.9)
$\Delta\varphi(\tau_1,\tau_2) < 175^o$	4.9×10^{-3} (96.4)	2.33×10^{-3} (98.0)	5.6×10^{-4} (83.9)
$E_{\nu_1,\nu_2} > 0$	2.0×10^{-3} (40.9)	9.60×10^{-4} (41.2)	2.1×10^{-4} (38.5)
N_{ev} at 30 fb^{-1}	60.3	28.8	6.4

% for the total uncertainty. The same uncertainty is used for the cross sections of the Wt and W+jet processes. The uncertainty of the $b\bar{b}Z/\gamma^*$ cross section measurement is estimated to be 14.2% in [144]. With these estimates, the total systematic uncertainty, including the luminosity uncertainty of 3% [7], was found to be 8.1%, 15.9%, 11.1%, 14.0% and 14.5% for the Z/γ^*, $b\bar{b}Z/\gamma^*$, $t\bar{t}$, Wt and W+jet backgrounds, respectively.

5.2.8.4 Discovery reach in the $M_A - \tan(\beta)$ plane.

Table 5.22 shows the number of signal plus background events and the number of background events for 30 fb^{-1} in the selected mass windows and the signal significance calculated according to Poisson statistics, with and without the background systematics taken into ac-

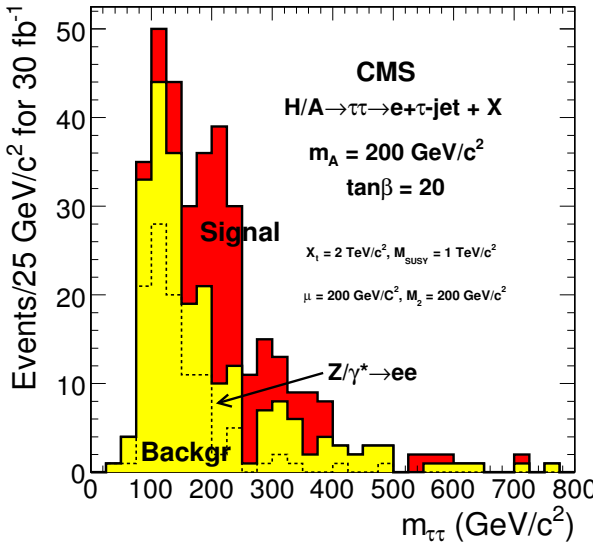

Figure 5.9: Reconstructed Higgs boson mass for the signal of $M_A = 200\,GeV/c^2$, $\tan\beta = 20$ and for the total background for an integrated luminosity of $30\,fb^{-1}$. The dashed line shows the sum of the $Z/\gamma^* \to e^+e^-$ and $b\bar{b}Z/\gamma^*e^+e^-$ backgrounds.

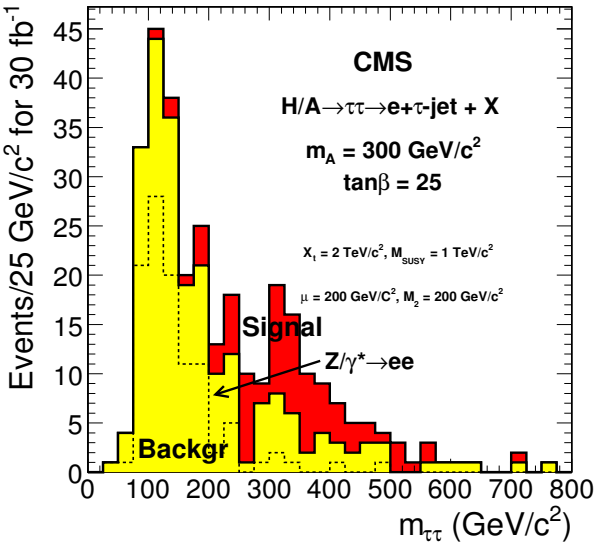

Figure 5.10: Reconstructed Higgs boson mass for the signal with $M_A = 300\,GeV/c^2$, $\tan\beta = 25$ and for the total background for an integrated luminosity of $30\,fb^{-1}$. The dashed line shows the sum of the $Z/\gamma^* \to e^+e^-$ and $b\bar{b}Z/\gamma^*e^+e^-$ backgrounds.

count. The mass windows were selected to optimise the significance. The m_h^{max} scenario was used.

Table 5.22: Number of signal-plus-background events and the number of background events in the selected mass windows for $30\,fb^{-1}$ and the signal significance without ($S_{no\ syst.}$) and with ($S_{syst.}$) the background systematics taken into account.

	$\Delta m_{\tau^+\tau^-}$	N_S+N_B	N_B	$S_{no\ syst.}$	$S_{syst.}$
$M_A = 130\,GeV/c^2$, $\tan\beta = 20$	120 - 200 GeV/c^2	176	83	8.9	6.4
$M_A = 140\,GeV/c^2$, $\tan\beta = 15$	130 - 220 GeV/c^2	136	76	9.1	6.7
$M_A = 200\,GeV/c^2$, $\tan\beta = 20$	140 - 280 GeV/c^2	175	83	8.8	6.3
$M_A = 300\,GeV/c^2$, $\tan\beta = 20$	240 - 480 GeV/c^2	78	39	5.4	4.3
$M_A = 500\,GeV/c^2$, $\tan\beta = 50$	360 - 780 GeV/c^2	57	22	6.2	5.3

Figure 5.11 shows the 5σ discovery region in the M_A-$\tan\beta$ plane for $30\,fb^{-1}$ in the m_h^{max} scenario, evaluated with and without background systematics.

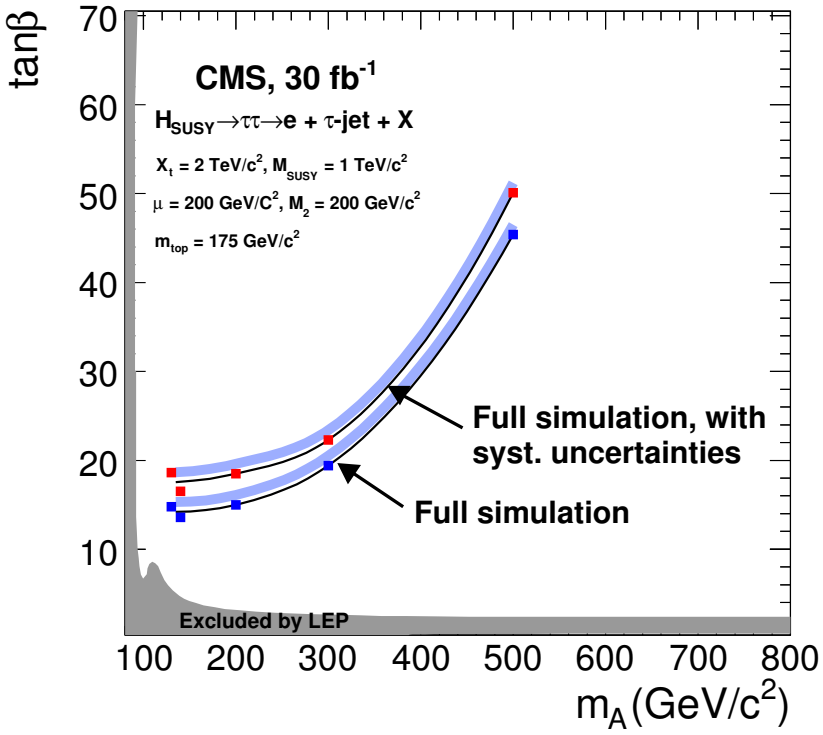

Figure 5.11: The 5σ discovery region in the $\mathrm{M_A}$-tan(β) plane for an integrated luminosity of 30 fb^{-1} in the $\mathrm{m_h^{max}}$ scenario. The lower (upper) curve was evaluated without (with) the effect of background systematics taken into account.

5.3 Benchmark Channels: $\mathrm{t\bar{t}H}$, $\mathrm{H} \rightarrow \mathrm{b\bar{b}}$

5.3.1 Introduction

The Higgs boson decay to $\mathrm{b\bar{b}}$ is the dominant mode for the Higgs mass range up to $m_H \sim 135\,\mathrm{GeV/c^2}$. Direct Higgs production is almost impossible to detect via this decay as a result of the combination of an overwhelming QCD cross section for $\mathrm{b\bar{b}}$ production and the inability to reconstruct the Higgs mass very precisely. While the latter is still true in the case of Higgs production in association with a $\mathrm{t\bar{t}}$ or $\mathrm{b\bar{b}}$ pair, these channels hold promise because they entail substantially lower backgrounds. The separation of these events into 3 salient topologies follows as a result of the ways in which the two W bosons in the event decay. Thus, in addition to the four b jets, roughly 49% of these events also contain four hadronic jets (the all-hadron channel), while some 28% have two hadronic jets together with an isolated electron or muon and missing E_t (the semi-leptonic channel), with a further 5% of events containing two oppositely-charged leptons (either of which can be an electron or muon) and missing E_t (the dilepton channel). The remaining 14% of events correspond to those cases where one or both of the W bosons decay to a tau lepton and neutrino and are not easily distinguishable as such, as a result of the rich decay repertoire of the tau meson. In fact, these events do make a small contribution to the three other classes of events in the actual analyses. Additional hadronic jets can appear in these events and originate from initial and final state QCD radiation (IFSR).

A detailed description of the $\mathrm{t\bar{t}H}$ analysis strategies and the results can be found in Reference [159]. All the results presented here are for an integrated luminosity of 60 fb^{-1}.

5.3.2 Event generation and simulation

As the identification of the signal relies upon the presence of top quark decay products, it comes as no surprise that the most significant backgrounds are those associated with $t\bar{t}$ events themselves. The main backgrounds are: $t\bar{t}jj$, $t\bar{t}b\bar{b}$ and $t\bar{t}Z$ with $Z \to b\bar{b}$.

These processes are studied in detail and are presented here. Secondary background sources include pure QCD multi-jet events in the case of the all-hadron channel, and W/Z plus jets or dibosons plus jets events in the case of the semi-leptonic and dilepton channels. With the exception of QCD multi-jets, the latter have substantially lower production cross-sections than $t\bar{t}$ events but very similar topologies. They are therefore not studied in detail.

Details about the primary Monte Carlo data samples used in this analysis are available in Reference [159]. The semi-leptonic and all-hadron $t\bar{t}H$ signal samples were generated using COMPHEP (version 41.10) and PYTHIA (version 6.215), while the dilepton samples used PYTHIA only. Though a leading order Monte Carlo, PYTHIA is known to do a very good job of reproducing IFSR as well as parton shower effects. This is adequate for the signal samples. For the $t\bar{t}$ plus jets backgrounds, greater care must be exercised. In particular, PYTHIA alone cannot be expected to do a realistic job since the relevant processes are not leading order. On the other hand, there is not currently a full next-to-leading order (NLO) MC for $t\bar{t}$ plus jets production. As a result, higher order matrix elements are used including additional radiated partons in conjunction with the parton showering of PYTHIA to produce the appropriate event topologies.

ALPGEN and PYTHIA are used for the matrix elements and parton showering, respectively, for the $t\bar{t}$ plus n jets background samples. The matching of the two generators is done in ALPGEN as discussed in Ref. [160]. In particular, all of the matrix elements for $t\bar{t}$ plus n additional hard partons are included and properly combined at each order taking into account the interference between amplitudes.

QCD events were generated with PYTHIA (version 6.215) in the $\hat{p}_t$ ranges from 120 to 170 GeV/c and greater than 170 GeV/c.

For the simulation of the interaction with the detector, the CMS tools, providing GEANT3 and GEANT4 based simulation of the CMS detector have been used.

The NLO signal cross-sections for different Higgs mass hypotheses are given in Table 5.23 together with the branching ratios for $H \to b\bar{b}$ [161].

The leading order COMPHEP cross-sections for the different background processes together with the effective cross-sections after the application of the generator filters are listed in Table 5.24. The ALPGEN cross sections for the different jet multiplicity processes are listed in

Table 5.23: NLO signal cross-sections and $H \to b\bar{b}$ branching ratios for different Higgs mass hypotheses

m_H	115 GeV/c^2	120 GeV/c^2	130 GeV/c^2
σ_{NLO} (pb)	0.747	0.664	0.532
$BR(H \to b\bar{b})$	0.731	0.677	0.525

Table 5.25. A detailed comparison of ALPGEN versus COMPHEP for the $t\bar{t}jj$ background is available in [159]. All the results that are presented here for the $t\bar{t}Nj$ backgrounds are based

Table 5.24: LO COMPHEP cross-sections and effective cross-sections after the generator filters of the considered background processes.

	QCD $\hat{p}_t$=120-170 GeV/c	QCD $\hat{p}_t$ >170 GeV/c	$t\bar{t}b\bar{b}$	$t\bar{t}Z$
σ_{LO} (pb)	$3.82{\cdot}10^5$	$1.05{\cdot}10^5$	3.28	0.65
$\sigma_{LO} \times \epsilon$ (pb)	76.4	336.0	2.82	0.565

Table 5.25: LO ALPGEN cross-sections for the different jet multiplicity samples.

	exclusive $t\bar{t}$+1j	exclusive $t\bar{t}$+2j	exclusive $t\bar{t}$+3j	inclusive $t\bar{t}$+4j
σ_{LO} (pb)	170	100	40	61

on the ALPGEN samples, where available.

5.3.3 Level-1 and high level trigger selections

A dedicated $t\bar{t}H$ trigger was not available and therefore was not implemented in the analysis. As a result, it is assumed in what follows that the signal is recorded by the CMS Level 1 (L1) and High Level Triggers (HLT) as described in [75]. Wherever possible, the cleaner signature of at least one isolated lepton in the final state is exploited. The semi-leptonic channels thus use the single muon (stream #43) or single electron (stream #2) triggers.

A logical "OR" of the single muon, single electron and single tau streams is used for the dilepton channel. The same trigger setups as for streams #43 and #2 were used, except that the p_T threshold was lowered to 15 GeV/c to permit selection of 20 GeV/c leptons later in the analysis. The tau trigger is the official stream (bit #91). Jet triggers are used to select all-hadron events. In particular, the single-jet, 3-jet and 4-jet triggers with low luminosity thresholds[75][162] are combined (stream #120 or #122 or #123).

Efficiencies for the various HLT and Level-1 triggers that were used are presented in Table 5.26. The efficiencies quoted are determined by counting the numbers of accepted events relative to the total numbers of events in each sample. In order to streamline the various studies that were performed, the analyses used different MC samples, produced with different final state constraints. Thus, efficiencies for single muon, single electron and fully hadronic final states were defined with respect to exclusive signal samples and inclusive background samples, as described in the preceding section. The dilepton channel efficiency on the other hand, was defined with respect to samples containing at least one leptonic top decay for the signal and inclusive samples for the backgrounds.

5.3.4 Reconstruction

5.3.4.1 Muon reconstruction

The process of muon reconstruction begins in the Muon Chambers and is then extended to the tracking system, as described in Ref. [163]. For the studies presented here it is important to identify muons coming from W decays. To this end, additional selection criteria are applied to distinguish these muons, which will be referred to as *signal* muons, from the muons coming from other sources such as b decays. The latter will be referred to as *background* muons, even though they arise in signal events as well as background events. The desired

Table 5.26: Signal and background efficiencies of the Level 1 and High Level Triggers.

	Single μ	Single e	Single e OR μ OR τ	Jets
$\mathrm{H} \to \mathrm{b\bar{b}}$ (%) with $m_H = 120\,\mathrm{GeV/c^2}$	63.5	52.4	76.7	24.9
$\mathrm{t\bar{t}b\bar{b}}$ (%)	19.0	16.1	83.6	18.3
$\mathrm{t\bar{t}}$1j (%)	13.9	11.3	53.0	2.9
$\mathrm{t\bar{t}}$2j (%)	14.0	11.1	59.8	6.2
$\mathrm{t\bar{t}}$3j (%)	14.0	11.1	68.5	11.4
$\mathrm{t\bar{t}}$4j (%)	13.4	11.1	78.6	31.4
$\mathrm{t\bar{t}Z}$ (%)	20.4	18.8	84.4	25.3
QCD 120-170 GeV/c (%)	0.08	0.8	4.3	1.7
QCD $> 170\,\mathrm{GeV/c}$ (%)	0.07	2.1	4.4	10.3

discrimination between *signal* and *background* muons is achieved by constructing a discriminator that is based upon probability density functions (PDF) for the following observables associated with muon candidates:

- Transverse momentum, p_t
- Track isolation, $IsoTk$
- Calorimeter isolation, $IsoCalo$
- Significance of track impact parameter, $S_{ip} = d/\sigma_d$

The PDF's associated with these variables for *signal* and *background* muons are obtained by matching to generator-level muons.

The PDF's are combined into the following likelihood ratio:

$$L = \Pi_i \frac{P_i^{sig}(x_i)}{P_i^{sig}(x_i) + P_i^{bkg}(x_i)} \tag{5.13}$$

where P_i^{sig} and P_i^{bkg} are the PDF's of an observable x_i for *signal* and *background* muons, respectively.

The performance for *signal* and *background* muon discrimination are shown in Figure 5.12. For a *signal* muon efficiency of 90%, only 1% of background muons are selected. The PDF's are constructed using a sample of $\mathrm{t\bar{t}H}$ events with $\mathrm{m_H} = 120\,\mathrm{GeV/c^2}$ in which one and only one of the W bosons decays to a muon and neutrino, while the other one decays hadronically.

If the likelihood selection is used after the HLT, a dramatic improvement in QCD ($\hat{p}_t > 170\,\mathrm{GeV/c}$) rejection is possible with little or no loss in signal efficiency. For example, a small drop in signal efficiency from 63% to 60% reduces the QCD efficiency by more than a factor of 3 (*i.e.* from 0.07% to 0.02%).

5.3.4.2 Electron reconstruction

A full description of the electron reconstruction in CMS can be found in Ref. [46]. Electrons coming from W boson decays are typically characterised by isolated high transverse energy clusters. These electrons are thus efficiently identified by means of an isolation requirement applied to the electron candidate with respect to other reconstructed tracks in the event.

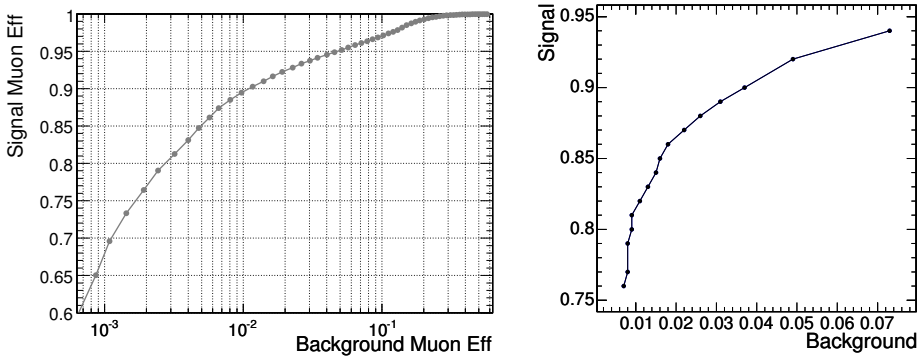

Figure 5.12: On the left: Performance of the muon likelihood discriminator for the semi-leptonic muon $\mathrm{t\bar{t}H}$ channel. On the right: $Signal$ versus $background$ electron efficiencies for likelihood values ranging from 0.006 (the upper point) with a step size of 0.006, (i.e. approximately in the range $1.0 < -\log(L_e) < 2.0$).

In analogy to the muon reconstruction and equation 5.13, a likelihood method is used to identify the signal electrons, making use of the following observables:

- the p_t sum of tracks inside an *isolation cone* of radius $\Delta R = 0.3$ around the candidate electron direction
- the ΔR distance between the electron candidate and the closest track
- the transverse momentum of the electron candidate, p_t
- the ratio between the cluster energy and the track momentum, E/p
- the ratio between the hadronic and electromagnetic energies of the cluster, H/E

An appropriate choice of likelihood cut value has been studied by comparing $signal$ versus $background$ electron efficiencies as shown in Figure 5.12.

For a $-Log(L_e)$ cut value of 1.27, $signal$ electrons are selected with an efficiency of 84% and $background$ electrons with an efficiency of 1.5%. This value was chosen for the analyses described in subsequent sections.

Concerning the efficiency of the likelihood cut with respect to background rejection in $\mathrm{t\bar{t}jj}$ events in which there were no isolated electrons coming from W decays, only 6% of these events were accepted for a likelihood cut of 1.27.

As in the case of the muon selection, the likelihood approach can be used to augment the HLT selection efficiency. Maintaining a roughly constant signal efficiency, the likelihood cut in combination with the HLT trigger yields an order of magnitude reduction in the QCD background selection efficiency.

5.3.4.3 Jet and missing E_{T} reconstruction

Jets are reconstructed using the iterative cone algorithm. A cone with ΔR = 0.5 is used when at least one W boson decays into leptons, while a smaller cone size was found to be more suitable for the more dense jet environments associated with the all-hadron channel (see below).

A calorimetric-tower energy threshold of 0.8 GeV and a transverse-energy threshold of 0.5 GeV are used. Calorimeter towers that exceed 1 GeV are considered as jet seeds. For the leptonic

channels, the jet energy is calibrated using MC calibrations [164] provided by the JetMET group for the corresponding set of reconstruction parameters.

The single lepton analyses, as described in more detail below, make use of an event likelihood to help select and properly reconstruct events and decay chains. This is facilitated, in part, by making use of the various invariant mass constraints associated with the top quark decays. The corresponding likelihoods thus rely upon the resolutions that are obtained for the invariant masses of the hadronically decaying W boson and the two top quarks. The "best-case" invariant mass distribution for the hadronically decaying top quark is reconstructed by matching to generator-level parton information and shown in Figure 5.13. The distributions for the leptonically decaying top quark and the hadronically decaying W boson (Ref. [159]) have similar shapes but different RMS (25.7 GeV/c^2 and 15.7 GeV/c^2, respectively) since the longitudinal momentum of the leptonically decaying top quark has to be calculated from missing E_t. A reconstructed jet is considered as matched to the corresponding parton if their separation, ΔR_{j-p}, is less than 0.3.

The missing transverse energy of the event E_t^{miss} is computed as

$$E_t^{miss} = \sum_i E_t^{tower} - (\sum_j E_t^{RawJet} - \sum_k E_t^{CaliJet}) + \sum_m E_t^{Muon} \tag{5.14}$$

where the sum with index i runs over calorimeter towers, that with index j runs over raw jets, k runs over calibrated jets, and m runs over the reconstructed muons of the event. Equation 5.14 thus takes into account the corrections due to jet calibration and the contributions of muons that are not measured in the calorimeter.

The choice of the jet reconstruction algorithm is an important step in the event selection optimisation for the all-hadron $\mathrm{t\bar{t}H}$ channel, where at least 8 jets are expected in the final state. For this reason, an optimisation is obtained by means of a simple "proto" analysis as described in Reference [159].

A dedicated $\mathrm{t\bar{t}H}$ calibration [165] is applied to help recover the original transverse energy of the associated parton. Reconstructed jets with a b-tagging discriminator value higher than 0.4 are calibrated using a separate b-jet calibration procedure.

Figure 5.13 shows the significance with respect to the S/N ratio for a range of b-tag discriminator values for each of the several cone sizes indicated. Lower discriminator values yield higher significance but only at the cost of low S/N while, on the contrary, higher discriminator values give lower significance but higher S/N. A good compromise is in the middle range of each of the curves where neither S/N nor significance are unreasonably low. With this in mind, the best choice for the jet cone is seen to be $\Delta R = 0.40$.

5.3.4.4 b-Tagging

The identification of jets from b-quarks is done with the *Combined Secondary Vertex* algorithm. This algorithm exploits secondary vertex and track properties to calculate a discriminator value which separates b-jets from non b-jets. A detailed description is published in Ref. [156] which also presents results of detailed studies of the performance of the b-tagging algorithm as applied to Monte Carlo $\mathrm{t\bar{t}}$ and QCD samples.

In the $\mathrm{t\bar{t}H}$ analyses, a fixed cut value for the b-tagging discriminator is applied, and four jets are required to pass this cut in the semi-leptonic and all-hadron channels, while only 3 jets are required to be tagged in the dilepton analysis. The misidentification rate of charm and

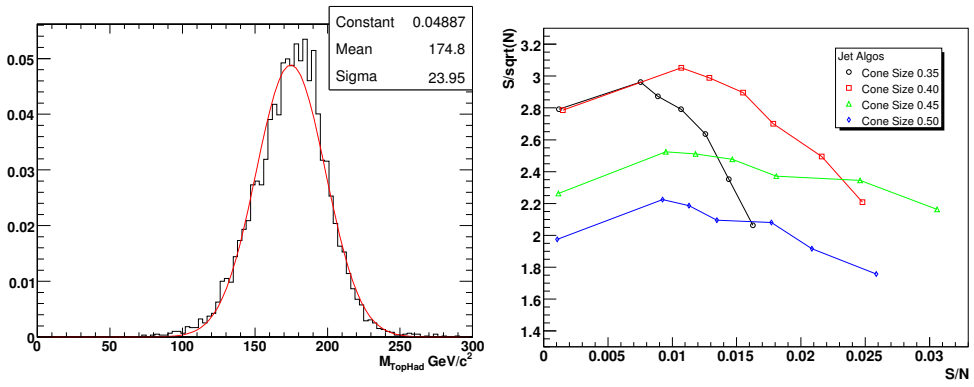

Figure 5.13: Left: Invariant mass of the hadronically decaying Top quark using jet-parton matching with $\Delta R_{j-p} < 0.3$. Right: Change in significance and S/N resulting from variations in the b-tagging discriminator for the various cone sizes indicated in the legend.

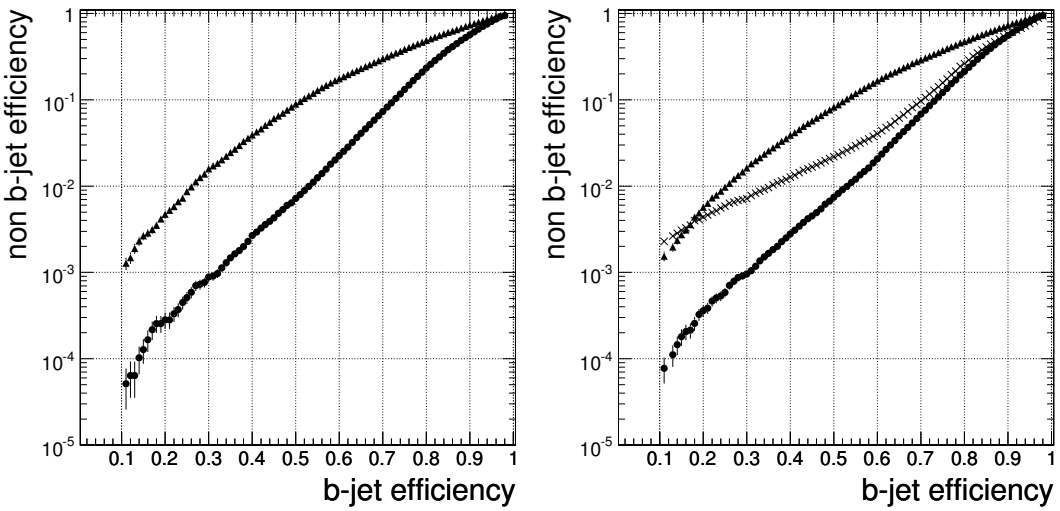

Figure 5.14: On the left: Non-b jet mistagging efficiency versus b-jet tagging efficiency for c-jets (triangles), and uds-jets (stars) for the $\mathrm{t\bar{t}H}$ sample with $m_H = 120\ \mathrm{GeV}/c^2$ and jets with a minimum transverse momentum of 20 GeV/c. For this plot the "physics definition" of the original jet flavour has been used. In this definition there are no original gluon jets in the $\mathrm{t\bar{t}H}$ sample. On the right: The corresponding plot for the $\mathrm{t\bar{t}jj}$ sample, where gluon jets are represented by crosses.

light flavour jets as a function of the b-tagging efficiency is shown in Fig. 5.14 for the $\mathrm{t\bar{t}H}$ and the $\mathrm{t\bar{t}jj}$ samples, respectively. It can be seen that the efficiencies are similar in these samples.

This fixed-cut b-tagging approach gives reasonable results, but is not necessarily optimal. Some potential improvements are possible such as the combination with a soft lepton tag or a discriminator cut which depends on p_t and η of the jets. Studies have shown that they have the potential to improve the results at the order of some percent. These improvements were not used in the current analyses.

5.3.5 Event selection

In this section the event selection for the different channels under consideration is described. In order to be able to combine the results from all the $\mathrm{t\bar{t}H}$ search channels, the different channels use mutually exclusive event samples. This is most easily facilitated by coordinating how high p_t electrons and muons from the W decays (previously referred to as $signal$ leptons) are either selected or vetoed by the different analyses.

For the analyses reported here, the different data samples used were separated using selection and/or veto criteria based on the lepton likelihood value, as described in Ref. [159].

5.3.5.1 Semi-leptonic Channel: $\mathrm{t\bar{t}H} \to \mathrm{b\bar{b}b\bar{b}qq'}\mu\nu_\mu$ and $\mathrm{b\bar{b}b\bar{b}qq'e}\nu_\mathrm{e}$

The strategy for selecting $\mathrm{t\bar{t}H}$ events with one isolated muon or electron in the final state can be summarised in the following three steps: pre-selection, choice of jet pairing and finally, selection. The pre-selection requires the HLT stream for a single muon or a single electron, one isolated lepton using the likelihood information as described in section 5.3.4.1 and 5.3.4.2, and 6 or 7 jets in the pseudorapidity region $|\eta| < 3.0$ with a calibrated transverse energy larger than 20 GeV. In order to recover some efficiency, jets with $10\,\mathrm{GeV} < E_t < 20\,\mathrm{GeV}$ are also accepted if they have at least two associated tracks pointing to the signal primary vertex [2] within a distance along the beam (z) axis of ($|z_{PV} - z_{track}| < 1$ mm). The latter condition is required to reject low transverse energy fake jets, (i.e. jets that are not associated with any of the signature partons in the signal event). For the single electron channel, the misidentification of the jet with the isolated electron has been excluded by imposing a veto on the jet if the electron lies inside a jet cone radius of 0.1.

At least 4 jets are required to be tagged as b-jets with a minimal discriminator value corresponding to a b-efficiency of about 70%.

To decrease the contamination from the dilepton channel, a double muon, double electron and muon-electron veto is applied, in which events with the second lowest $-\log(L_\mu) < 1.4$ and events with $-\log(L_e) < 1.2$ are rejected from the analysis. In the case of the semi-leptonic electron channel the previous cuts are applied respectively to the first muon likelihood candidate and to the second electron likelihood candidate. The application of these vetoes results in a lowering of the signal efficiency by about 2%, while the total background rejection is increased by 13%.

In order to perform a complete reconstruction of the event, the longitudinal momentum of the neutrino has to be computed from four-momentum conservation for the W boson: $m_W^2 = (E^\mu + E^\nu)^2 - (\vec{p}^{\,\mu} + \vec{p}^{\,\nu})^2$. This equation gives 2 real solutions for p_z^ν in 66% of the cases, while in the remaining 34%, the neutrino is assumed to be collinear with the lepton: $p_z^\nu = p_z^l$. This leads to a small degradation in the longitudinal momentum resolution, but the reconstruction efficiency of the leptonic W boson decay is increased to 100%.

In order to choose the jet combination that does the best job of reconstructing the two top quarks, a likelihood, L_{Event}, is defined using masses, b-tagging and kinematic information from the whole event:

$$L_{Event} = L_{Mass} \times L_{bTag} \times L_{Kine}. \tag{5.15}$$

The mass information considered in the likelihood L_{Mass} is the probability returned by the kinematic fit with invariant mass constraints (top quarks and hadronic W) that is described

[2] The signal interaction is generally the one which allows the event to be triggered.

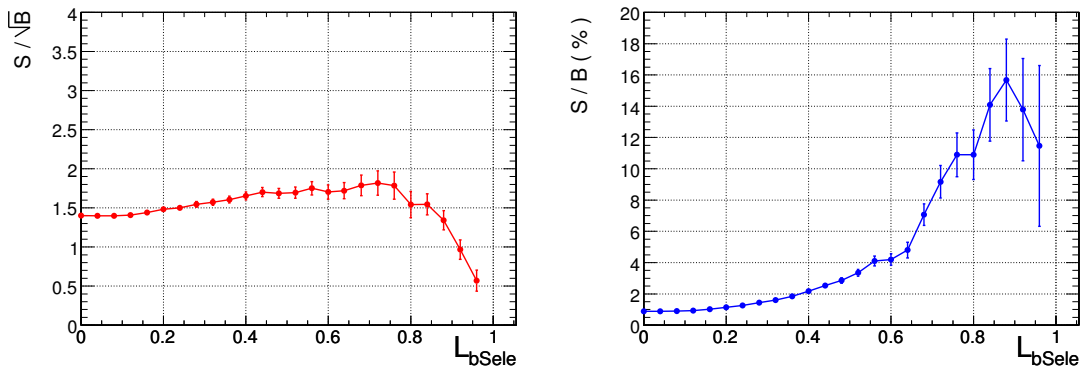

Figure 5.15: $\mathrm{t\bar{t}H}$ ($W \to qq', W \to \mu\nu$): Signal Significance (left) and Signal to Background ratio (right) as function of the cut on L_{bSele}.

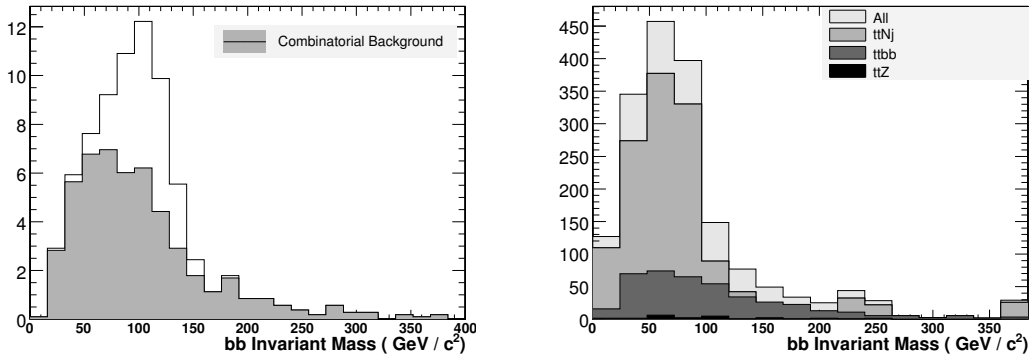

Figure 5.16: $\mathrm{t\bar{t}H}$ ($W \to qq', W \to \mu\nu$). Left: Invariant $b\bar{b}$ mass for signal only (combinatorial background is shaded grey). Right: The sum of the reconstructed $m_{b\bar{b}}$ spectra for backgrounds with a value of $L_{bSele} > 0.55$. The distributions are normalised to an integrated luminosity of 60 fb^{-1}.

in Reference [166].

The b-tagging function L_{bTag} is defined as the product of the b-tag discriminators: $L_{bTag} = D_{Top_{Had}} \times D_{Top_{Lep}} \times D_{H_1} \times D_{H_1} \times (1 - D_{W1}) \times (1 - D_{W2})$; where Top_{Had} and Top_{Lep} are expected to be the two b jets from the hadronic and leptonic top, respectively, while H_1 and H_2 are expected to be the two b jets coming from Higgs and W_1 and W_2 are the two jets from the hadronically-decaying W boson.

The kinematic function takes into account the observation that the b-jets coming from top quarks tend to be slightly more energetic than b-jets coming from the Higgs boson (see [159] for a definition).

Among all possible combinations of jet-parton assignments, the one with the highest value of L_{Event} is chosen for use in the final reconstruction of the top quarks and the two remaining jets with highest b-tagging discriminator values are used to reconstruct the Higgs mass.

After the jet assignment is complete, additional criteria are applied to improve background rejection. In particular, a stronger b-tag requirement is applied on the event variable $L_{bSele} = D_{Top_{Had}} \times D_{Top_{Lep}} \times D_{H_1} \times D_{H_2}$.

The signal significance as a function of the selection cut L_{bSele} is shown in Figure 5.15.

The distributions of reconstructed Higgs mass for the final selected events are shown in Figure 5.16 for signal only (left) and for the combination of the different backgrounds (right) for the muon channel only (similar results for the electron channel can be found in [159]). The fraction of signal events where the two b-jets are correctly assigned to the Higgs boson (i.e. the pairing efficiency) is roughly 31% in the muon channel and about 29% for the electron channel.

5.3.5.2 Results

The selection efficiencies with the corresponding numbers of expected events and signal significances are reported in Table 5.27 for the channels with a muon or an electron in the final state. The number of expected events is computed for an integrated luminosity of 60 fb^{-1} in the Standard Model Higgs mass range from 115 to 130 $\mathrm{GeV/c^2}$.

5.3.5.3 Dilepton channel: $\mathrm{t\bar{t}H} \to \mathrm{b\bar{b}b\bar{b}}\ell'\nu'\ell\nu$

Dilepton $\mathrm{t\bar{t}H}$ events are selected by requiring two reconstructed leptons (e,μ) accompanied by significant missing transverse energy and at least four but no more than seven jets, at least three of which have been b-tagged according to the *Combined Secondary Vertex* b-tagging algorithm.

Lepton identification is performed using the electron and muon likelihoods described in Section 5.3.4. In the semi-leptonic analyses, events with more than one identified lepton are vetoed, but in the dilepton analysis those events are retained. The likelihood acceptance cuts used for leptons in the dilepton channel are therefore chosen to be the same as the second-lepton veto cuts for both semi-leptonic channels. In this way, the sample of events for the dilepton $\mathrm{t\bar{t}H}$ analysis is by construction strictly complementary to those used in the semi-leptonic channels.

The details of the dilepton $\mathrm{t\bar{t}H}$ selection are summarised below:

- 2 oppositely-charged leptons (e,μ) passing identification criteria ($-\log(L_\mu) < 1.4$ for muons, $-\log(L_e) < 1.2$ for electrons)
- corrected $E_T^{\mathrm{miss}} > 40\,\mathrm{GeV}$
- 4 to 7 jets with calibrated $E_T > 20\,\mathrm{GeV}$ and $|\eta| < 2.5$
- $\geq$3 selected jets b-tagged with discriminator $D > 0.7$

The above is termed the "loose" working point because there is evidence that it is possible to increase the purity (S/B) of the selection, by way of more stringent criteria:

- 4 to 6 jets with calibrated $E_T > 20\,\mathrm{GeV}$ and $|\eta| < 2.5$
- $\geq$4 selected jets b-tagged with discriminator $D > 0.7$

The generated W^- was forced to decay leptonically (e, μ, τ), but the W^+ was allowed to decay freely. This "non-exclusive" dataset incurs a branching ratio of $1/3$, which has been factored into the selection efficiencies reported in Table 5.28. This choice allows us to obtain a good estimate of the overlap of the contribution to the dilepton sample arising from semi-leptonic top decays which are mis-reconstructed as dilepton events; the same applies to tau decays which are mis-reconstructed as e, μ.

The background events have small efficiency to pass the selection criteria, so very large samples must be analysed. To make these samples more manageable, a loose pre-selection re-

Table 5.27: Selection efficiency for $L_{bSele} > 0.55$ (ϵ_{loose}) and for $L_{bSele} > 0.75$ (ϵ_{tight}), number of expected events and signal significance in 60 fb^{-1} for the muon and electron $\mathrm{t\bar{t}H}$ channel. The numbers refer to the complete Higgs mass range.

muon channel					
	Analysed Ev.	ϵ_{loose} (%)	N^{ev}_{loose} 60 fb^{-1}	ϵ_{tight} (%)	N^{ev}_{tight} 60 fb^{-1}
$\mathrm{t\bar{t}H}$ (115)	27768	2.00 ± 0.08	96 ± 4	0.80 ± 0.05	38 ± 3
$\mathrm{t\bar{t}H}$ (120)	41929	1.90 ± 0.07	75 ± 3	0.74 ± 0.04	29 ± 2
$\mathrm{t\bar{t}H}$ (130)	19466	2.23 ± 0.11	55 ± 3	0.84 ± 0.07	21 ± 2
$\mathrm{t\bar{t}b\bar{b}}$	372737	0.247 ± 0.008	419 ± 14	0.0877 ± 0.0048	148 ± 8
$\mathrm{t\bar{t}1j}$	393000	0.0051 ± 0.0011	520 ± 120	0.00076 ± 0.00044	78 ± 45
$\mathrm{t\bar{t}2j}$	568999	0.0105 ± 0.0014	633 ± 82	0.00070 ± 0.00035	42 ± 21
$\mathrm{t\bar{t}3j}$	101000	0.0050 ± 0.0022	119 ± 53	0.	$< 27 (68\% C.L)$
$\mathrm{t\bar{t}4j}$	86697	0.0035 ± 0.0020	126 ± 73	0.	$< 48 (68\% C.L.)$
$\mathrm{Zt\bar{t}}$	50000	0.068 ± 0.012	23 ± 4	0.026 ± 0.007	9 ± 2
Total Background			1840		< 352
$S/\sqrt{B}$ (115)			2.2		2.0
S/B (115)			5.1%		10.8%
$S/\sqrt{B}$ (120)			1.8		1.6
S/B (120)			4.1%		8.2%
$S/\sqrt{B}$ (130)			1.3		1.1
S/B (130)			3.0%		6.0%

electron channel					
	Analysed Ev.	ϵ_{loose} (%)	N^{ev}_{loose} 60 fb^{-1}	ϵ_{tight}	N^{ev}_{tight} 60 fb^{-1}
$\mathrm{t\bar{t}H}$ (115)	27692	1.39 ± 0.07	66 ± 3	0.52 ± 0.04	25 ± 2
$\mathrm{t\bar{t}H}$ (120)	42228	1.42 ± 0.06	56 ± 2	0.53 ± 0.04	21 ± 1
$\mathrm{t\bar{t}H}$ (130)	19127	1.57 ± 0.09	39 ± 2	0.61 ± 0.06	15 ± 1
$\mathrm{t\bar{t}b\bar{b}}$	372737	0.176 ± 0.007	297 ± 12	0.0641 ± 0.0041	109 ± 7
$\mathrm{t\bar{t}1j}$	393000	0.0038 ± 0.0010	390 ± 100	0.00025 ± 0.00025	26 ± 26
$\mathrm{t\bar{t}2j}$	568999	0.0067 ± 0.0011	401 ± 65	0.00123 ± 0.00046	74 ± 28
$\mathrm{t\bar{t}3j}$	101000	0.0040 ± 0.0020	95 ± 48	0.	$< 27 (68\% C.L)$
$\mathrm{t\bar{t}4j}$	86697	0.0023 ± 0.0016	84 ± 60	0.	$< 48 (68\% C.L.)$
$\mathrm{Zt\bar{t}}$	50000	0.064 ± 0.011	22 ± 4	0.022 ± 0.007	7 ± 2
Total Background			1289		< 291
$S/\sqrt{B}$ (115)			1.8		1.5
S/B (115)			5.1%		8.6%
$S/\sqrt{B}$ (120)			1.6		1.2
S/B (120)			4.4%		7.2%
$S/\sqrt{B}$ (130)			1.1		0.9
S/B (130)			3.0%		5.2%

quiring at least 3 b-tags with discriminator $D > 0.7$ is applied before analysis.

5.3.5.4 Results

The selection efficiencies for the two working points, with the corresponding number of expected events and the signal significance, are reported in Tables 5.28. The number of expected events is computed for an integrated luminosity of 60 fb^{-1}.

Since the event selection is quite simple for the dilepton channel, it is possible to formulate

Table 5.28: Selection efficiency ϵ_{loose} (including branching fraction where applicable) and resulting number of expected events N_{loose} in 60 fb^{-1}, for the dilepton $\mathrm{t\bar{t}H}$ channel. For a glimpse of possible improvements, the same for a tighter set of cuts is provided (ϵ_{tight}, N_{tight}). Also quoted are binomial errors arising from the finite sizes of processed datasets. The $\mathrm{t\bar{t}H}$ datasets are labelled by the generated Higgs mass in GeV/c^2 (parentheses).

	#analysed	$\epsilon_{loose}(\%)$	N^{ev}_{loose}	$\epsilon_{tight}(\%)$	N^{ev}_{tight}
$\mathrm{t\bar{t}H}$ (115)	27900	0.511 ± 0.025	168 ± 8	0.088 ± 0.010	29 ± 3
$\mathrm{t\bar{t}H}$ (120)	26141	0.490 ± 0.025	132 ± 7	0.070 ± 0.009	19 ± 3
$\mathrm{t\bar{t}H}$ (130)	25911	0.490 ± 0.025	82 ± 4	0.072 ± 0.010	12 ± 2
$\mathrm{t\bar{t}b\bar{b}}$	313894	0.637 ± 0.014	1080 ± 24	0.094 ± 0.007	159 ± 12
$\mathrm{t\bar{t}}$1j	280385	0.0125 ± 0.0021	1270 ± 220	0	< 42 (68% C.L.)
$\mathrm{t\bar{t}}$2j	276917	0.0448 ± 0.0040	2690 ± 240	0.00144 ± 0.00072	87 ± 43
$\mathrm{t\bar{t}}$3j	90367	0.0553 ± 0.0078	1330 ± 190	0	< 31 (68% C.L.)
$\mathrm{t\bar{t}}$4j	12281	0.0716 ± 0.0077	2620 ± 280	0.0025 ± 0.0014	92 ± 53
$\mathrm{t\bar{t}Z}$	110156	0.304 ± 0.017	103 ± 6	0.0363 ± 0.0057	12 ± 2
all backgrounds			9090		< 422
$S/\sqrt{B}$ (115)			1.8		1.4
S/B (115)			1.8 (%)		6.9 (%)
$S/\sqrt{B}$ (120)			1.4		0.9
S/B (120)			1.5 (%)		4.5 (%)
$S/\sqrt{B}$ (130)			0.9		0.6
S/B (130)			0.9 (%)		2.9 (%)

simple equations predicting the selection efficiencies. This is detailed in Ref. [159], where some back-of-the-envelope calculations to estimate these efficiencies for both signal and backgrounds are presented, including some of the backgrounds that were not taken into account in this analysis.

5.3.5.5 All-hadron channel: $\mathrm{t\bar{t}H} \to \mathrm{b\bar{b}b\bar{b}qq'q''q'''}$

A number of kinematic variables, together with the b-tagging discriminator, have been studied to optimise the signal selection with respect to background rejection. Moreover, in order to combine the results from the 4 different decay sub-channels, a veto on leptons has been applied using the complementary cut developed within the semi and fully leptonic decays analyses: events are discarded if $-\log(L_\mu) < 1.4$ or $-\log(L_e) < 1.2$.

The final set of variables that are used in this analysis is the following:

- Jet Transverse Energy of the 8 most energetic jets in the tracker acceptance
- Combined b-Tag discriminator variable for each jet
- Centrality of the event defined as $\sum_{i=0}^{8} E_T^i / E^i$
- Centrality of the Higgs defined similarly, with the sum restricted to the 2 jets paired to the Higgs

The jet-to-parton matching is performed using a χ^2 method as defined in [159].

Two working points have been chosen: the first uses loose cuts on the b-tagging discriminator to get higher statistical significance (but lower S/B), while the second uses a tighter cut on the b-tagging discriminator to obtain a higher S/B (but lower significance). For the first

working point an event is selected if the following conditions are satisfied:

- $E_T^{7th} > 30\,\text{GeV}$ and $E_T^{8th} > 20\,\text{GeV}$ for the E_T ordered jets
- the χ^2 for each of the 2 W bosons and 2 t quarks are within 3 sigma of their expected values
- the 3 highest combined b-tagging discriminators for the 4 jets associated to the b-partons must satisfy $D_3 > 0.80$
- Higgs centrality higher than 0.55 and no cut on Event Centrality

For the tight working point, the b-tagging discriminator for the third highest jet is required to satisfy $D_3 > 0.85$ and the fourth one $D_4 > 0.70$, while the event and Higgs centrality are required to exceed 0.55 and 0.80, respectively.

All the applied cuts have been optimised to obtain the highest significance while keeping the S/B ratio as high as possible. All values chosen for E_T^{7th}, E_T^{8th}, D_3, D_4, Event and Higgs centrality have been varied simultaneously, thereby mapping out the complete set of combinations within the following limits:

- $20\,\text{GeV} < E_T^{8th} < 40\,\text{GeV}$
- $E_T^{8th} < E_T^{7th} < E_T^{8th} + 40\,\text{GeV}$
- $0.5 < D_3$ and $D_4 < 0.95$
- Event and Higgs Centrality in the range [0.50-0.95]

Variation of more than one cut has also been tested and the final implemented set of cut values is that for which significance and S/B are optimal.

5.3.5.6 Results

The number of analysed events, selection efficiencies with the corresponding number of expected events and the signal significance are reported in Tables 5.29 for the all-hadron decay channel. Both working points are considered.

5.3.6 Discussion of systematic uncertainties

5.3.6.1 Estimation of "standard" CMS systematics

The uncertainties in various quantities, given the knowledge of the CMS experiment at the time of writing this note, are considered first. These differ from what they are expected to be after CMS has collected 60 fb^{-1} of data.

In keeping with other CMS analyses, the following "standard" sources of systematic error are considered:

- Jet energy scale (JES) (3% to 10% depending on p_t)
- Jet resolution (10%)
- b-jet and c-jet tagging efficiencies (4%)
- uds-jet tagging efficiencies (10%)
- Luminosity (3%)

It is assumed that the systematics listed above are uncorrelated. Each source is varied independently which produces a change in the selection efficiency $\Delta\epsilon$ and the corresponding

Table 5.29: Analysed events, selection efficiency, number of expected events and signal significance in 60 fb^{-1} for the all-hadron $\mathrm{t\bar{t}H}$ channel for 2 different working points: ϵ_{loose} and ϵ_{tight}. The numbers refer to the full mass range.

	#analysed	$\epsilon_{loose}(\%)$	N^{ev}_{loose} 60 fb^{-1}	$\epsilon_{tight}(\%)$	N^{ev}_{tight} 60 fb^{-1}
$\mathrm{t\bar{t}H}$ (115)	49636	2.32 ± 0.07	347 ± 10	0.294 ± 0.015	44 ± 4
$\mathrm{t\bar{t}H}$ (120)	163494	2.55 ± 0.04	314 ± 5	0.366 ± 0.024	45 ± 2
$\mathrm{t\bar{t}H}$ (130)	43254	2.80 ± 0.08	214 ± 6	0.358 ± 0.029	27 ± 2
$\mathrm{t\bar{t}bb}$	203135	0.702 ± 0.019	1190 ± 31	0.0645 ± 0.0056	109 ± 9
$\mathrm{t\bar{t}1j}$	1031551	0.0084 ± 0.0009	860 ± 92	0.0005 ± 0.0002	49 ± 22
$\mathrm{t\bar{t}2j}$	559111	0.0333 ± 0.0024	2000 ± 150	0.0009 ± 0.0004	54 ± 24
$\mathrm{t\bar{t}3j}$	68015	0.079 ± 0.011	1910 ± 260	0.0015 ± 0.0015	35 ± 35
$\mathrm{t\bar{t}4j}$	97334	0.182 ± 0.014	6660 ± 500	0.0021 ± 0.0015	75 ± 53
$\mathrm{Zt\bar{t}}$	80226	0.358 ± 0.021	121 ± 7	0.0312 ± 0.0062	11 ± 2
qcd170	264310	0.0238 ± 0.0030	4810 ± 610	0.0004 ± 0.0004	76 ± 76
qcd120	55128	0.0018 ± 0.0018	83 ± 83	0 ± 0	$<95(68\% C.L.)$
Total Backgr.			17600		< 505
$S/\sqrt{B}$ (115)			2.6		2.0
S/B (115)			2.0%		8.7 %
$S/\sqrt{B}$ (120)			2.4		2.0
S/B (120)			1.8%		8.9 %
$S/\sqrt{B}$ (130)			1.6		1.2
S/B (130)			1.2%		5.4 %

change in expected event yields ΔN_X ($X = \mathrm{t\bar{t}H}, \mathrm{t\bar{t}1j}, ...$) for the signal and background.

A very detailed breakdown of the various sources of systematic uncertainties and the methods of how they are computed for all the background and signal samples is available in Reference [159]. In Tables 5.30, the systematic uncertainties are propagated to the expected signal significance for "tight" and "loose" working points.

5.3.6.2 Background rates from data

There are relatively large theoretical uncertainties in the cross-sections used to normalise the signal yields [161], and even larger theoretical uncertainties in those used for the $t\bar{t}$+jets backgrounds [167]. These have not been included as part of the systematic errors considered above, because when the CMS experiment reaches maturity, estimating the $\mathrm{t\bar{t}}$+jets background directly from data ought to be possible. In this way, the uncertainty associated with Monte Carlo derived tagging rates are avoided entirely. For example, the number of mistagged $\mathrm{t\bar{t}}$+jets which can be factorised as follows:

$$N^{mistag}_{t\bar{t}jj} = N^{no-tag}_{t\bar{t}jj} \times Pr(uds \to b; E_T, \eta, ...)$$

where $N^{no-tag}_{t\bar{t}jj}$ is a high purity (e.g. fully reconstructed with a mass window) top sample that has been obtained without requiring b-tagging and $Pr(uds \to b; E_T, \eta, ...)$ is a parameterised "fake matrix" that is derived from some independent dataset (*e.g.* dijet data) which yields the probability for a light quark jet to fake a secondary vertex. It may also be possible to derive this fake matrix from the top sample itself. If a high-purity (e.g. double-tagged and fully reconstructed) semi-leptonic top sample were selected, the jets belonging to the hadronic W would provide a source of both light quark and charm jets. From these data, a

Table 5.30: Significance before and after taking into account the uncertainty dB in the total number of background events due to systematics.

muon	S/B	$S/\sqrt{B}$	$S/\sqrt{B+dB^2}$
$L_{bSele} > 0.55$ (ϵ_{loose})			
$t\bar{t}H$ (115)	0.052	2.2	0.20
$t\bar{t}H$ (120)	0.041	1.8	0.15
$t\bar{t}H$ (130)	0.030	1.3	0.11
$L_{bSele} > 0.75$ (ϵ_{tight})			
$t\bar{t}H$ (115)	0.108	2.0	0.44
$t\bar{t}H$ (120)	0.082	1.6	0.34
$t\bar{t}H$ (130)	0.060	1.1	0.24

dilepton	S/B	$S/\sqrt{B}$	$S/\sqrt{B+dB^2}$
4-7 jets, 3-4 b-tagged (ϵ_{loose})			
$t\bar{t}H$ (115)	0.018	1.8	0.10
$t\bar{t}H$ (120)	0.015	1.4	0.08
$t\bar{t}H$ (130)	0.009	0.9	0.05
4-6 jets, 4-6 b-tagged (ϵ_{tight})			
$t\bar{t}H$ (115)	0.069	1.4	0.42
$t\bar{t}H$ (120)	0.045	0.9	0.27
$t\bar{t}H$ (130)	0.029	0.6	0.18

electron	S/B	$S/\sqrt{B}$	$S/\sqrt{B+dB^2}$
$L_{bSele} > 0.55$ (ϵ_{loose})			
$t\bar{t}H$ (115)	0.051	1.8	0.20
$t\bar{t}H$ (120)	0.044	1.6	0.17
$t\bar{t}H$ (130)	0.030	1.1	0.12
$L_{bSele} > 0.75$ (ϵ_{tight})			
$t\bar{t}H$ (115)	0.086	1.5	0.37
$t\bar{t}H$ (120)	0.072	1.2	0.31
$t\bar{t}H$ (130)	0.052	0.9	0.22

hadron	S/B	$S/\sqrt{B}$	$S/\sqrt{B+dB^2}$
Working Point ϵ_{loose}			
$t\bar{t}H$ (115)	0.020	2.6	0.07
$t\bar{t}H$ (120)	0.018	2.4	0.07
$t\bar{t}H$ (130)	0.012	1.6	0.05
Working Point ϵ_{tight}			
$t\bar{t}H$ (115)	0.087	2.0	0.22
$t\bar{t}H$ (120)	0.089	2.0	0.22
$t\bar{t}H$ (130)	0.054	1.2	0.13

measurement of the corresponding uds-tag and c-tag rates at the relevant energy could be directly obtained.

5.3.7 Combined significance

Since the event samples for the channels studied in this note are strictly disjoint, the results can be combined by simply adding the individual signal yields (background yields) to obtain a summed S (B).

For each of the considered systematics, the resultant error in background yields are added for all four channels, since they are by definition fully correlated. The summed errors are then added by quadratures to get a combined systematic uncertainty dB. One then calculates the significance, inclusive of systematic uncertainties in the background yield, according to the formula $S/\sqrt{B+dB^2}$.

It is of interest to see how much better the results have the potential to be at tighter working points for the various analyses. Since the systematic uncertainties are not well quantified at these "tight" working points, because of a lack in Monte Carlo Statistics, the same uncertainties as for the "loose" working points are used to reduce spurious statistical effects. This procedure can be justified by the observation that the impact of the b-tagging and uds-mistagging uncertainty is smaller at the "tight" working points and the JES uncertainty becomes dominant. Since the "tight" working points are defined by stronger b-tagging cuts, while keeping the E_T cuts constant, no major change in the relative systematic uncertainty is expected. A more detailed study of the systematic error at the "tight" working points for samples with enough Monte Carlo Statistics is available in Ref. [159].

It is difficult to predict at this time exactly what will be the level to which the backgrounds can be understood, because the tools required are not yet in existence and because this understanding requires real data. In view of this, it is interesting to consider how the combined significance of the measurements presented in this note would vary as a function of the fractional uncertainty in background cross-sections, i.e. as dB_{xsec}/B.

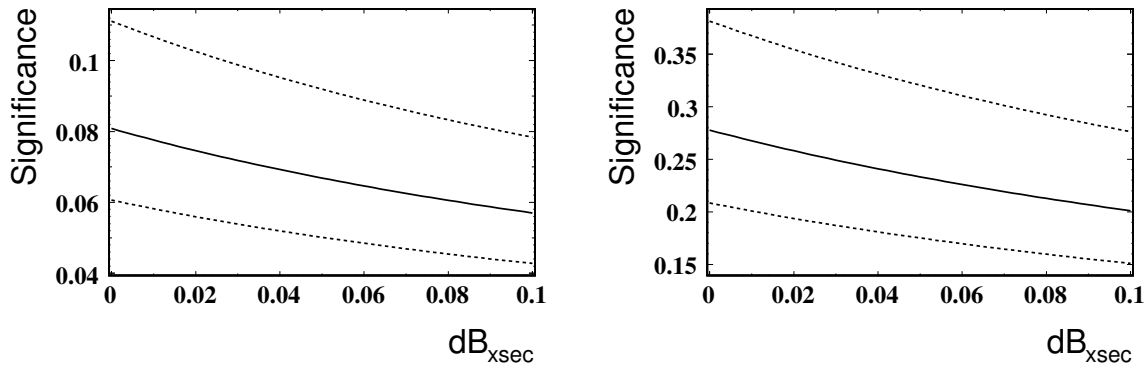

Figure 5.17: Expected range of combined significance (dilepton + semi-leptonic + all-hadron, and includes the systematic uncertainties estimated in Section 5.3.6.1) versus an additional systematic uncertainty on the background cross-section as a fraction of total background. Left: Results for the "loose" working points. Right: Results for the "tight" working points.

The solid central line in Figure 5.17 shows how the combined significance $S/\sqrt{B + (dB_{sys} + dB_{xsec})^2}$ degrades as a function of dB_{xsec}/B. The signal and background yields for the tightest working points (N^{ev}_{tight} in Table 5.27, Table 5.28 and Table 5.29) are used in the right side of Figure 5.17, because these give the best results after inclusion of systematics.

Other than this "fundamental" cross-section uncertainty, there is also the "correctible" errors in the cross-sections used at the time of writing, which can be compensated for once data has been collected. The upper and lower dashed curves in Figure 5.17 show the maximum and minimum allowed excursions, should the signal and background cross-sections be off by 10% and 20% respectively. Thus the upper (lower) dashed line corresponds to the signal cross-section scaled up (down) by 10% while at the same time the background cross-section is scaled down (up) by 20%.

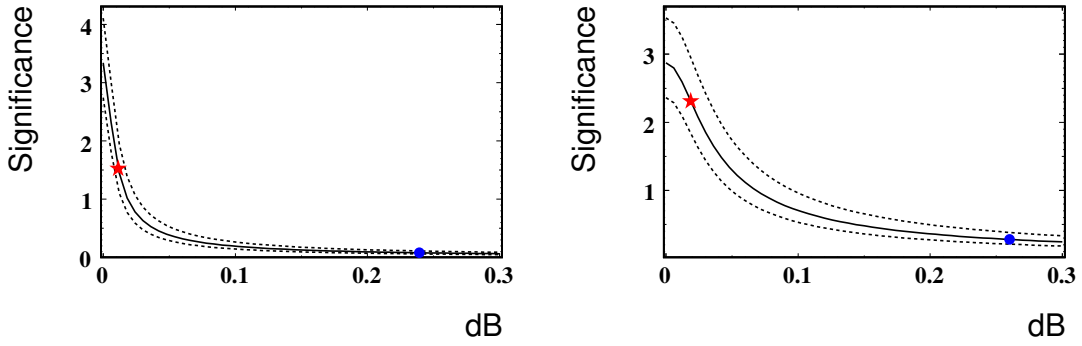

Figure 5.18: Expected range of combined significance (dilepton + semi-leptonic + all-hadron) versus the total systematic uncertainty in background as a fraction of total background. Left: Results for the "loose" working points. Right: Results for the "tight" working points.

It is also of interest to see how much better the analyses could do if the total systematic uncertainty can be reduced (i.e. the region left of zero in Figure 5.17). Hence, Figure 5.18 shows the full range of obtainable significances, with the dot marking the currently estimated value with no cross-section uncertainty ($dB = dB_{sys}$). The star corresponds to what one would obtain for 1% and 4% uncertainties on the $t\bar{t}$Nj and $t\bar{t}b\bar{b}$ backgrounds, respectively, an arbitrarily chosen reference. It is interesting to note that it does not quite yield a substantial

significance, even though background uncertainties of 1% and 4% for $\mathrm{t\bar{t}Nj}$ and $\mathrm{t\bar{t}b\bar{b}}$ are probably substantially better than what will be accessible in reality. This highlights the challenge that is faced in observing $\mathrm{t\bar{t}H}$.